

University of Kentucky

UKnowledge

Theses and Dissertations--Electrical and
Computer Engineering

Electrical and Computer Engineering


2020

EXPANDED PREDICTIVE EQUATION FOR DC ARC-FLASH INCIDENT ENERGY IN 125V BATTERY SYSTEMS

Austin Gaunce

University of Kentucky, acga227@uky.edu

Author ORCID Identifier:

 <https://orcid.org/0000-0002-6734-4727>

Digital Object Identifier: <https://doi.org/10.13023/etd.2020.117>

[Right click to open a feedback form in a new tab to let us know how this document benefits you.](#)

Recommended Citation

Gaunce, Austin, "EXPANDED PREDICTIVE EQUATION FOR DC ARC-FLASH INCIDENT ENERGY IN 125V BATTERY SYSTEMS" (2020). *Theses and Dissertations--Electrical and Computer Engineering*. 148. https://uknowledge.uky.edu/ece_etds/148

This Master's Thesis is brought to you for free and open access by the Electrical and Computer Engineering at UKnowledge. It has been accepted for inclusion in Theses and Dissertations--Electrical and Computer Engineering by an authorized administrator of UKnowledge. For more information, please contact UKnowledge@lsv.uky.edu.

STUDENT AGREEMENT:

I represent that my thesis or dissertation and abstract are my original work. Proper attribution has been given to all outside sources. I understand that I am solely responsible for obtaining any needed copyright permissions. I have obtained needed written permission statement(s) from the owner(s) of each third-party copyrighted matter to be included in my work, allowing electronic distribution (if such use is not permitted by the fair use doctrine) which will be submitted to UKnowledge as Additional File.

I hereby grant to The University of Kentucky and its agents the irrevocable, non-exclusive, and royalty-free license to archive and make accessible my work in whole or in part in all forms of media, now or hereafter known. I agree that the document mentioned above may be made available immediately for worldwide access unless an embargo applies.

I retain all other ownership rights to the copyright of my work. I also retain the right to use in future works (such as articles or books) all or part of my work. I understand that I am free to register the copyright to my work.

REVIEW, APPROVAL AND ACCEPTANCE

The document mentioned above has been reviewed and accepted by the student's advisor, on behalf of the advisory committee, and by the Director of Graduate Studies (DGS), on behalf of the program; we verify that this is the final, approved version of the student's thesis including all changes required by the advisory committee. The undersigned agree to abide by the statements above.

Austin Gaunce, Student

Dr. Joseph Sottile, Major Professor

Dr. Aaron Cramer, Director of Graduate Studies

EXPANDED PREDICTIVE EQUATION FOR
DC ARC-FLASH INCIDENT ENERGY IN 125V BATTERY SYSTEMS

THESIS

A thesis submitted in partial fulfillment of the
requirements for the degree of Master of Science in Electrical Engineering in the
College of Engineering
at the University of Kentucky

By

Austin Cody Gaunce

Lexington, Kentucky

Director: Dr. Joseph Sottile, Professor of Mining Engineering

Lexington, Kentucky

2020

Copyright © Austin Cody Gaunce 2020
<https://orcid.org/0000-0002-6734-4727>

ABSTRACT OF THESIS

EXPANDED PREDICTIVE EQUATION FOR DC ARC-FLASH INCIDENT ENERGY IN 125V BATTERY SYSTEMS

Arc-flash is a dangerous phenomenon that can occur during an arcing fault in an electrical system. People nearby may be subjected to extreme heat, light, pressure, and sound. Research regarding arc-flash has focused primarily on AC arc-flash due to the prevalence of AC electricity in the grid. However, the grid has begun to integrate more DC electrical sources as a result of decentralization efforts and environmental concerns. The increased proliferation of DC electrical sources demands research into DC arc-flash to assess the hazard as low-voltage DC sources have already become commonplace. Some DC arc-flash models have been produced to estimate incident energy. These models are either theoretical or semi-empirical in nature, as empirical research pertaining to DC arc-flash is scarce. The lack of empirical DC arc-flash data inspired a series of tests at American Electric Power's (AEP's) Dolan Technology Center (DTC) that were conducted in August 2018. These tests allowed the development of a limited empirical equation for incident energy. The research presented in this thesis is a continuation of the August 2018 DC arc-flash testing with the objective of generating an expanded incident energy equation. Furthermore, this research seeks to address the effects of some atmospheric conditions on the behavior of low-voltage DC arcs.

KEYWORDS: Arc Flash, DC Arc Flash, Electrical Safety, Incident Energy, Batteries

Austin Cody Gaunce

(Name of Student)

02/22/2020

Date

EXPANDED PREDICTIVE EQUATION FOR
DC ARC-FLASH INCIDENT ENERGY IN 125V BATTERY SYSTEMS

By
Austin Cody Gaunce

Joseph Sottile

Director of Thesis

Aaron Cramer

Director of Graduate Studies

02/22/2020

Date

ACKNOWLEDGMENTS

First and foremost, I would like to thank my wife, Elizabeth Gaunce, for her love and support throughout this endeavor. Without her, I doubt this thesis would have come to fruition. In addition, I would like to thank my friends and family for their compassion and encouragement. The completion of this thesis would also not have been possible without the help of my academic advisor, Joseph Sottile, who has helped guide me through two theses while I have attended the University of Kentucky.

I would also like to thank my co-workers and leadership at American Electric Power (AEP) for the thoughtful discussions and support that allowed this DC arc-flash testing to happen in the first place. I would like to specifically thank Ron Wellman, my supervisor, for his support and understanding while I have been writing this thesis; and Xuan Wu, my fellow arc-flash subject master expert (SME), for bringing my attention to arc-flash and his mentorship, and Dennis Hoffman for his help gathering the supplies that allowed the DC arc-flash tests to proceed. Furthermore, I would like to thank John Mandeville, Dave Klinect, Anthony “Tony” Clarke, Surya Baktiono, Chase Leibold, Darvin Williams, Amrit Khalsa, and everyone else at the Dolan Technology Center (DTC) for all their help with testing, from building the test setup to executing the test plan. I look forward to working with you all on future research projects.

TABLE OF CONTENTS

ACKNOWLEDGMENTS	iii
LIST OF FIGURES	vi
LIST OF TABLES	viii
CHAPTER 1 : INTRODUCTION	9
1.1 Statement of the Problem.....	9
1.2 Scope of Work	9
CHAPTER 2 : LITERATURE REVIEW	11
2.1 Introduction to Arc-flash.....	11
2.2 Arc-flash Standards.....	11
2.2.1 IEEE 1584.....	12
2.2.2 NFPA 70E.....	13
2.3 Evolution of the Electric Utility Industry and DC Arc-flash Sources	13
2.4 DC Arc-flash Models.....	15
2.4.1 Doan Model	15
2.4.2 Ammerman Model.....	16
2.4.3 Multiplication Factor Model	17
2.4.4 DC Arc Magnetohydrodynamic (MHD) Model	18
2.5 DC Arc-flash Testing.....	18
2.5.1 Kinectrics	19
2.5.2 Bonneville Power Administration.....	19
2.5.3 American Electric Power	20
2.5.4 Hydro-Quebec.....	21
2.6 Chapter Summary	22
CHAPTER 3 : METHODOLOGY	23

3.1 Testing Arrangement and Equipment	23
3.2 Test Setups	27
3.3 Testing Procedure	29
CHAPTER 4 : DATA ANALYSIS	33
4.1 Gap Width Analysis.....	33
4.1.1 Relationship between Gap Width and Maximum Temperature Rise	33
4.1.2 Relationship between Gap Width and Arc Characteristics.....	34
4.1.3 Relationship between Gap Width and Arc Energy	39
4.2 Working Distance Analysis	43
4.3 Arc Current Analysis	45
4.4 Weather Data Analysis	48
4.4.1 Relative Humidity.....	48
4.4.2 Temperature	50
4.4.3 Air Pressure.....	52
4.4.4 Multiple Linear Regression.....	53
4.5 Chapter Summary	53
CHAPTER 5 : MODEL DEVELOPMENT	56
5.1 Discussion of DC Arc-flash Test Stage 1 Model.....	56
5.2 Development of DC Arc-flash Test Stage 2 Model.....	56
5.3 Cross-Validation and Refinement of DC Arc-flash Test Stage 2 Model.....	63
5.4 Model Comparison.....	65
CHAPTER 6 : CONCLUSION AND FUTURE WORK.....	66
APPENDIX.....	68
REFERENCES	75
VITA.....	77

LIST OF FIGURES

Figure 3.1: Power Schematic of Testing Arrangement [23]	24
Figure 3.2: Test Enclosure in Environmental Chamber [23]	25
Figure 3.3: Environmental Chamber and Dehumidifier Controls [23]	26
Figure 4.1: Gap Width and Max Temperature Rise Relationship for Battery 2 & 3	33
Figure 4.2: Gap Width and Max Temperature Rise Relationship for Battery 3	34
Figure 4.3: Example of Decreasing Arc Power (Power 250R26(9))	35
Figure 4.4: Example of Parabolic Arc Power (Power 125R4(5))	35
Figure 4.5: Example of Increasing Arc Power (Power 062R26(1))	36
Figure 4.6: Initial Arc Current vs. Gap Width for Batteries 2 & 3	37
Figure 4.7: Initial Arc Current vs. Gap Width for Battery 3	37
Figure 4.8: Initial Arc Voltage vs. Gap Width for Batteries 2 & 3	38
Figure 4.9: Initial Arc Voltage vs. Gap Width for Battery 3	38
Figure 4.10: Initial Arc Resistance vs. Gap Width for Batteries 2 & 3	39
Figure 4.11: Initial Arc Resistance vs. Gap Width for Battery 3	39
Figure 4.12: Comparison of Original and Smoothed Signals	40
Figure 4.13: Arc Energy vs. Gap Width for Batteries 2 & 3	40
Figure 4.14: Arc Energy vs. Gap Width for Battery 3	41
Figure 4.15: Example of Typical Power Transfer Curve	42
Figure 4.16: Simple Circuit for Power Transfer Example	42
Figure 4.17: Left Portion of Power Transfer Example	43
Figure 4.18: Right Portion of Power Transfer Example	43
Figure 4.19: Max Temperature Rise vs. Working Distance for Stage 1 Tests	44
Figure 4.20: Max Temperature Rise vs. Working Distance for Stage 2 Tests	44
Figure 4.21: Comparison of Stage 1 and Stage 2 Working Distance Relationships	45
Figure 4.22: Max Temperature Rise vs. Initial Arc Current for a 1/16-inch Gap Width ..	46
Figure 4.23: Max Temperature Rise vs. Initial Arc Current for a 1/8-inch Gap Width ...	46
Figure 4.24: Max Temperature Rise vs. Initial Arc Current for a 1/4-inch Gap Width ...	47
Figure 4.25: Max Temperature Rise vs. Initial Arc Current for a 1/2-inch Gap Width ...	47
Figure 4.26: Average Arc Currents vs. Gap Width	48

Figure 4.27: Arc Duration vs. Relative Humidity at Medium Temperature.....	49
Figure 4.28: Arc Duration vs. Relative Humidity at High Temperature	50
Figure 4.29: Arc Duration vs. Relative Humidity at Low Temperature.....	50
Figure 4.30: Arc Duration vs. Temperature at Medium Relative Humidity.....	51
Figure 4.31: Arc Duration vs. Temperature at High Relative Humidity	52
Figure 4.32: Arc Duration vs. Temperature at Low Relative Humidity.....	52

LIST OF TABLES

Table 3.1: Summary of Testing Equipment	27
Table 3.2: DC Arc-flash Stage 2 Test Setups - Planned	28
Table 3.3: DC Arc-flash Stage 2 Test Setups - Revised	29
Table 3.4: Summary of Testing Procedure	32
Table 4.1: Arc Duration vs. Humidity Regression Results at Various Temperature Levels	49
Table 4.2: Arc Duration vs. Temperature Regression Results at Various Humidity Levels	51
Table 4.3: Arc Duration vs. Air Pressure Regression Results	53
Table 5.1: Statistical Analysis Summary of Incident Energy Models	59
Table 5.2: Summary of Model 1, 2, and 3 Accuracy Measurements.....	59
Table 5.3: Summary of Results for Arc Current vs. Bolted Fault Current, Gap Width, and Interaction Term.....	61
Table 5.4: Summary of Results for Arc Energy vs. Arc Current and Gap Width	61
Table 5.5: Summary of Results for Incident Energy vs. Arc Energy and Working Distance.....	61
Table 5.6: Summary of Results for Arc Current vs. Bolted Fault Current, Gap Width, and Interaction Term.....	62
Table 5.7: Summary of Results for Normalized Incident Energy vs. Arc Energy	62
Table 5.8: Summary of Results for Incident Energy vs. Working Distance at a Gap Width of 0.125 Inches	62
Table 5.9: Summary of Model A, B, C, and D Accuracy Measurements	63
Table 5.10: Summary of Cross-Validation Results	64
Table 5.11: Summary of Results for Refined Arc Energy vs. Bolted Fault Current, Gap Width, and Interaction Term.....	64
Table 5.12: Summary of Results for Refined Normalized Incident Energy vs. Arc Energy	64
Table 5.13: Summary of Refined Model D Accuracy Measurements.....	65
Table 5.14: Model Comparison Summary	65

CHAPTER 1: INTRODUCTION

1.1 Statement of the Problem

DC arc-flash is poised to become a greater hazard in the electric utility industry as more DC sources such as solar panels and energy storage systems are integrated into the grid. Even though there may be greater risk in the future, DC arc-flash hazards exist today. Battery systems are commonly employed by electric utilities to maintain operation of critical communication and control devices in substations in during power failures. The size of these battery installations vary based on the scale of the substation. Research pertaining to DC systems trails research in AC systems. Several models have been proposed to address arc-flash hazards in DC systems. These models are either theoretical or semi-empirical in nature, as there is little empirical DC arc-flash data available. IEEE 1584, the industry standard regarding arc-flash hazard calculations, lacks an equation for DC systems due in part to the lack of empirical research. Ultimately, more empirical research is needed to improve the body of knowledge surrounding DC arc-flash, produce more accurate equations, and develop effective mitigation strategies.

In August of 2018, a series of DC arc-flash tests were performed at American Electric Power's (AEP's) Dolan Technology Center (DTC) [1], [2]. (These tests will be referred to as Stage 1 tests in this thesis.) The test setup was placed outside of the building due to fire concerns. On August 8th, there was difficulty sustaining arcs despite previous success using similar configurations. It was hypothesized that atmospheric conditions may have been influencing the sustainability of the arcs [2]. A second series of tests were proposed where the test setup would be moved inside the building and placed in an environmental chamber. This chamber allowed temperature conditions to be controlled. In addition, control of relative humidity was achievable with the attachment of an industrial dehumidifier. Besides addressing atmospheric conditions, an additional battery was acquired for the second test stage. The new battery was 125 V_{DC} with a capacity of 400 Ah, making it the largest battery acquired for testing; therefore, testing was planned to refine and expand upon the model previously established by the August 2018 tests [1], [2].

1.2 Scope of Work

The primary objective of this research is to build upon previous research conducted by AEP to refine a predictive equation for estimating incident energy levels from substation battery backup systems utilized in AEP's footprint. The acquisition of a larger battery (400 Ah) allows current to be an independent variable for testing and an expanded model that includes gap width, working distance, and current can be created. A secondary objective of this research is to assess the influence of atmospheric conditions on arc sustainability.

Flooded lead-acid batteries with 125 V_{DC} nominal voltage levels served as the source of the test system. Furthermore, system fault current levels encountered during

testing ranged from approximately 3800 A to 5900 A. Testing focused on the following variables: gap width (inches), working distance (inches), battery fault current (amps), temperature (degrees Fahrenheit), and relative humidity (percent). Gap width values employed include 0.063 (1/16) inches, 0.13 (1/8) inches, 0.25 (1/4) inches, and 0.50 (1/2) inches. Working distances assessed include 6 inches, 9 inches, 12 inches, and 15 inches. Temperature and relative humidity were divided into three levels each. Temperature levels were comprised of 32 degrees Fahrenheit, 68 degrees Fahrenheit (or approximate room temperature), and 85 degrees Fahrenheit. Relative humidity levels used for testing were 20%, 40% and 80%.

CHAPTER 2: LITERATURE REVIEW

2.1 Introduction to Arc-flash

An arc-flash occurs when there is an arcing fault in an electrical system in the presence of people. Heat is the hazard commonly associated with arc-flash; however, harmful levels of pressure, light, and sound may be produced as well. The arc produced during an arc-flash incident can reach a temperature of 35,000 degrees Fahrenheit at its terminals [3]. Furthermore, lethal burns can occur at several feet from high-current arcs with severe burn injuries possible even at 10 feet [3]. Incident energy is the quantification of thermal energy a person may be exposed to at a specific distance. The unit of measure for incident energy is calories per square centimeter (cal/cm^2).

Arc-flash and electrocution/shock are two hazards commonly associated with electrical systems. Out of the two hazards, electrocution/shock is more recognizable by the general public. However, arc-flash possesses a significant risk to electrical workers with an estimated 5 to 10 arc-flash explosions occurring every day in the United States [4]. In 2018, 160 fatalities and 1560 nonfatal incidents could be attributed to electricity. No fatal injuries were attributed to electrical burns whereas 490 nonfatal injuries were due to electrical burns. The construction industry possessed the highest incident rate for fatalities due to electricity (0.8 per 100,000 people) with 54% of all electrical fatalities occurring in the construction industry for 2018. The industry with the second highest incident rate for electrical fatalities was the utility industry (0.55 per 100,000 people) [5].

Electrical burn injuries are not solely due to arc-flash. Arc-flash is not independently tracked; therefore, statistics on arc-flash rely upon additional research and corroboration from multiple sources (e.g., Bureau of Labor Statistics injury data, OSHA reports, research regarding burn treatment centers). Further research reveals that arc-flash is a key contributor, accounting for a significant number of electrical burn injuries [6]. Moreover, based on research into a Texas burn center, exposure to arc-flash produced larger burns than other burn sources with a mean length of stay of 11.3 days [7].

2.2 Arc-flash Standards

In the United States, there are two standards that provide advice regarding arc-flash hazards: IEEE 1584 and NFPA 70E. The Institute of Electrical and Electronics Engineers (IEEE) manages IEEE 1584, which provides guidance regarding the calculation of incident energy calculations. The National Fire Protection Agency (NFPA) manages NFPA 70E, which provides recommended work practices to specify arc-flash PPE and arc boundaries. Arc boundaries establish minimum PPE requirements at specified distances from a piece of equipment. The distance used by an arc boundary is defined by incident energy estimates. In addition, NFPA 70E defines the different levels of arc-flash PPE and the arc rating associated with each PPE level.

2.2.1 IEEE 1584

IEEE 1584 was first published in 2002 as a culmination of years of research (arc-flash-specific research began in 1982 with the publication of “The Other Electrical Hazard: Electric Arc Blast Burns” by Ralph H. Lee). The equations provided by the 2002 standard were developed as a result of more than 300 tests [8]. These equations were limited to the following system parameters [9]:

- Three-phase AC electrical faults
- System voltages of 208 V to 15,000 V
- System frequencies of 50 Hz or 60 Hz
- Bolted fault currents ranging from 700 A to 106,000 A
- Grounded or ungrounded systems
- Common equipment enclosure sizes
- Conductor gap widths ranging from 13 mm to 152 mm

For systems above 15 kV or gap widths outside the applicable range, IEEE 1584-2002 includes the Lee method. The Lee method is expressed by (1).

$$E = (2.142 \times 10^6)VI_{bf} \left(\frac{t}{D^2} \right) \quad (1)$$

where:

E = incident energy (J/cm^2)

V = system voltage (kV)

t = arc duration (s)

D = working distance (mm)

I_{bf} = bolted fault current (kA)

The equations provided by IEEE 1584-2002 served industry for 16 years before the publication of the 2018 edition of IEEE 1584. IEEE 1584-2018 provides updated equations derived from approximately 2000 additional arc-flash tests [8]. The new equations have an expanded range of applications stemming from testing using different bolted fault currents, gap widths, working distances, and electrode configurations. Accounting for different electrode configurations is one of the most significant changes between the two versions of IEEE 1584. In IEEE 1584-2002, all tests were performed using a vertical arrangement. For testing within an enclosure, the electrodes were funneled through holes in the roof of the box. Furthermore, no test arrangement included an insulating barrier. In IEEE 1584-2018, the IEEE 1584-2002 electrode arrangements were termed VCB (vertical electrodes in an enclosure or box) and VOA (vertical electrodes in open air). In addition, three new arrangements were included in IEEE 1584-2018: VCBB (vertical electrodes in a box with an insulating barrier); HCB (horizontal

electrodes in a box); and HOA (horizontal electrodes in open air). Note that while IEEE 1584-2018 expanded significantly upon the work in IEEE 1584-2002, IEEE 1584-2018 is still only applicable to three-phase faults in AC systems. Single-phase AC faults and DC faults remain outside the scope of IEEE 1584. For faults in DC systems, IEEE 1584-2018 directs attention to a series of research papers published regarding DC arc-flash for guidance.

2.2.2 NFPA 70E

The NFPA 70E standards development committee was established in 1976 at the request of the Occupational Safety and Health Administration (OSHA) with the objective of addressing electrical safety for employees. Prior to the establishment of the NFPA 70E committee, OSHA relied upon the National Electrical Code (NEC) for regulating electrical installations to mitigate hazards. The failure of the NEC to address employee safety is the primary reason for the formation of the NFPA 70E committee [10]. Approximately three years after the formation of the NFPA 70E committee, the first edition of NFPA 70E was published. Arc-flash hazards were not part of the scope of NFPA 70E until 1995 [11].

Since its establishment, NFPA 70E has served to guide electrical safety practices with OSHA acting as the federal authority for the enforcement of safety regulations. Regulations pertaining to electrical safety are captured by Subpart S of Title 29 of the Code of Federal Regulations (CFR). The CFR utilizes more general language than NFPA 70E; therefore, the NFPA 70E is typically used by employers to establish protective measures against electrical hazards [11].

NFPA 70E primarily addresses arc-flash PPE and labeling requirements; however, some guidance is provided regarding the performance of arc-flash hazard calculations. As of the seventh edition, these calculations are contained in Annex D of NFPA 70E. Note that these equations are for informational purposes [10]. Therefore, incident energy calculations are addressed by other standards and research. In addition, NFPA 70E provides recommendations on the frequency that arc-flash studies should be reviewed. As of the 2018 publication of the NFPA 70E, arc-flash studies should be reviewed (and updated if necessary) every five years.

2.3 Evolution of the Electric Utility Industry and DC Arc-flash Sources

The “War of the Currents” established the fundamental groundwork that would define the electric utility industry. At the conclusion of the “War of the Currents,” AC electricity became the basis of the electric transmission and distribution system. AC electricity has proven itself as an effective means of transferring electrical power over great spans of distance. The traditional model of the electric utility industry is centralized because of the nature by which electricity is produced and distributed. Historically, electricity has been produced at large power plants that rely upon different fuel sources such as coal, uranium, and natural gas, or water (in the case of hydroelectric plants). From these power plants, voltage was stepped up to level at a neighboring substation and

then transferred to end-users through the series of wires that comprise the transmission, subtransmission, distribution, and utilization systems.

This centralized model has served the electric utility industry since its inception; however, recent industry trends have seen a shift towards a decentralized model. A decentralized industry model distributes electricity generation from a few large power plants to numerous small generators that are in close-proximity to the end-user. This transition has been spurred partly by environmental concerns regarding the pollution associated with the use of fossil fuels. Solar and wind energy are two clean energy sources that have started to supplant traditional fossil fuel power plants. Both of these energy sources can be deployed on a large scale, similar to traditional power plants (e.g., solar farms, wind farms) or on a small scale as a distributed energy resource (DER) (e.g., rooftop solar panels, personal wind turbines). The transition to wind and solar energy has come at the cost of increased uncertainty in the reliability of the electric grid due to their intermittent nature. Therefore, energy storage systems (ESSs), such as batteries, have been proposed to counteract some of the variance caused by solar and wind energy sources. Solar photovoltaic (PV) panels and batteries produce DC electricity. As the electric utility industry continues to deploy more of these technologies, the risk of DC arc-flash will become more prevalent.

Though ESSs are discussed in the previous section as a proposed solution to the intermittent qualities of solar and wind energy, one type of ESS has already been widely deployed by numerous industries: batteries. The type of battery that has been widely deployed possesses a low-voltage level, while medium and high voltage battery installations are rarer. Low-voltage batteries have been utilized by the electric utility industry for backup substation power to allow relays and protective equipment to continue operations during outage situations. Similarly, the telecom and technology industries utilize low voltage battery installations as backup power for data centers. Lastly, the automotive industry is another example of an industry with a large deployment of batteries due to electric vehicles. Therefore, low-voltage batteries are a present day risk of DC arc-flash in numerous industries.

Beyond solar panels and batteries, there is a third common source of DC arc-flash: rectifiers. A rectifier is a piece of equipment that converts AC electricity into DC electricity. A household example of a rectifier would be the charging/power block for a laptop battery charger. Rectifiers are a common component of battery systems due to chargers; however, they have also been used to tie separate electrical grids together. In the continental United States, there are three regions that compose the electrical grid: the western interconnection, the eastern interconnection, and the Texas interconnection. These three regions are tied together by rectifiers and inverters. This arrangement is due to frequency variance among the three regions. The US standardized at 60 Hz for AC electricity; however, there is some variation among frequency due to differences in system loading, generation dispatch, and different generation portfolios.

2.4 DC Arc-flash Models

There are a number of DC arc-flash models that have been proposed since the creation of IEEE 1584-2002. The 2018 version of IEEE 1584 does not provide an incident energy equation for DC electrical systems; however, IEEE 1584-2018 does explicitly mention several proposed DC arc-flash models for guidance. The standard does not recommend any single DC arc-flash model; therefore, the engineer is responsible for selecting a model to use. This section will discuss six different DC arc-flash models.

2.4.1 Doan Model

The Doan model was created by Dan Doan and published in IEEE Transactions on Industry Applications in 2010 [12]. This model was developed using a simple Thevenin equivalent circuit and is therefore a theoretical model. A key assumption of this model is maximum power transfer. The maximum power transfer theorem states that the maximum amount of power is transmitted to a load when the source and load resistances are equivalent. Another way of stating this theorem is that maximum power transfer occurs when the voltage of the load is half the source voltage. The assumption of maximum power transfer produces a conservative means for calculating incident energy. In addition, the Doan model was designed for open-air arcs. Therefore, the model does not account for the concentration effect of an enclosure on incident energy. To address this issue, Doan states that other literature determined that incident energy could be three times greater when an enclosure is present [12]. To account for different working distances, Doan employs the Inverse Square Law. The Inverse Square Law states that the energy emitted by a source decays at a rate of the distance (from the source) squared. The mathematical expression of this relationship is stated in (2).

$$E_D \propto \frac{1}{D^2} \quad (2)$$

where:

E_D = energy at some distance from the source

D = distance from the energy source

This relationship typically applies when the energy disperses in a spherical shape. Therefore, the previous mathematical expression is modified to account for the surface area of a sphere. Lastly, Doan assumes a linear relationship with time to accommodate for different arc durations. By using these various assumptions, Doan produces (3) [12].

$$IE_{\max power} = 0.005 \left(\frac{V_{sys}^2}{R_{sys}} \right) \left(\frac{T_{arc}}{D^2} \right) \quad (3)$$

where:

$IE_{\max power}$ = incident energy at maximum power transfer (cal/cm²)

V_{sys} = system voltage (V)

R_{sys} = system resistance (Ω)

T_{arc} = arc duration (s)

D = working distance (cm)

Equation (3) represents the final form of the Doan model. The coefficient (0.005) accounts for the 4π associated with the surface area of a sphere and the conversion factor 0.239 cal/J to convert the energy of the arc from joules to calories to obtain the traditional measurement unit of incident energy, cal/cm² [12].

2.4.2 Ammerman Model

The Ammerman model was developed by Ravel F. Ammerman, Tammy Gammon, P. K. Sen, and John P. Nelson and was published in IEEE Transactions on Industry Applications in 2010 (the same year and journal as the Doan model) [13]. The Ammerman model is considered a semi-empirical model due to the use of past empirical DC arc research. At the turn of the 20th century, arcs were being considered for lighting applications. Early research focused on determining the static characteristics of DC arcs. This research produced various voltage-current (V-I) relationships [13]. Ammerman et al. utilizes the V-I relationship proposed by Stokes and Oppenlander to solve for the resistance of a DC arc. The V-I relationship proposed by Stokes and Oppenlander is expressed by (4) and was developed via extensive testing of vertical and horizontal DC arcs produced by electrodes placed in series [14].

$$V_{arc} = (20 + 0.534z_g)I_{arc}^{0.12} \quad (4)$$

where:

V_{arc} = arc voltage (V)

z_g = gap width (mm)

I_{arc} = average arc current (A)

Rewriting (4) to solve for arc resistance produces (5), which is a crucial component of the Ammerman model [13]. Calculating arc resistance is an iterative process.

$$R_{arc} = \frac{20 + 0.534z_g}{I_{arc}^{0.88}} \quad (5)$$

where:

R_{arc} = arc resistance (Ω)

The second component of the Ammerman model is arc energy. Arc energy is defined in (6). Equation (6) is calculated using the arc resistance found via (5).

$$E_{arc} = I_{arc}^2 R_{arc} t_{arc} \quad (6)$$

where:

E_{arc} = arc energy (J)

t_{arc} = arc duration (s)

With arc energy, incident energy can then be calculated using (7) for open-air arcs or (8) for arcs in an enclosure. Equation (8) is based on the work of Wilkins [15].

$$E_s = \frac{E_{arc}}{4\pi d^2} \quad (7)$$

where:

E_s = incident energy of an open-air arc (J/mm²)

d = working distance (mm)

$$E_1 = k \frac{E_{arc}}{a^2 + d^2} \quad (8)$$

where:

E_1 = incident energy of an enclosed arc (J/mm²)

a = constant defined by enclosure dimensions (mm)

k = constant defined by enclosure dimensions (dimensionless)

After determining incident energy, a conversion is required, as the Ammerman model does not directly solve for incident energy in cal/cm². To convert J/mm² to cal/cm², multiply by 23.9.

2.4.3 Multiplication Factor Model

The Multiplication Factor model was formed by Michael Fontaine and Peter Walsh [16]. This model followed the work of Doan and Ammerman et al. As discussed in 2.4.1, the Doan model does not account for the presence of an enclosure. Therefore, the addition of a multiplication factor addresses this limitation. The multiplication factor is derived from the work of Wilkins (similar to the Ammerman model) [15]. Equation (9) defines the multiplication factor using (7) and (8).

$$M_f = \frac{E_1}{E_s} = \frac{k4\pi}{1 + (a/d)^2} \quad (9)$$

where:

M_f = multiplication factor (dimensionless)

Thus, a multiplication factor can be calculated based on the equipment enclosure size and the working distance from the arc. If working distance is unknown, then an iterative procedure can be used to determine the multiplication factor and ultimate arc-flash boundary distance. (Fontaine and Walsh use the value 1.2 cal/cm² to specify an arc-flash boundary [16].) Equation (10) is one of the arc-flash boundary equations proposed by Fontaine and Walsh (different equations were proposed based on the desired units of the arc-flash boundary, such as feet versus inches) [16].

$$D_{afb} = (0.000614(M_f)(V_{sys})(I_{bf})(T_{arc}))^{0.5} \quad (10)$$

where:

D_{afb} = arc-flash boundary distance (in)

V_{sys} = system voltage (V)

I_{bf} = system bolted-fault current to the fault location (A)

In addition, Fontaine and Walsh provide a series of figures that provide optimum values for a and k . These figures allow the interpolation of optimum values of a and k for equipment enclosure sizes that differ from the common dimensions specified in IEEE 1584-2002 [16].

2.4.4 DC Arc Magnetohydrodynamic (MHD) Model

In 2016, a MHD model was proposed for determining arc-flash hazards in DC electrical systems by Shiuan-Hau Rau, Zhenyuan Zhang, and Wei-Jen Lee [17]. This model leverages advances in computer simulation to model DC arc physics. Magnetohydrodynamics is a field of research that combines electromagnetics and fluid mechanics to simulate how electromagnetic fields behave around a moving fluid (plasma). The computations required for MHD modeling are intensive and require the use of computers to solve within a reasonable timeframe. A series of assumptions were used in the development of the DC Arc MHD model [17]:

1. The arc plasma is considered a continuous fluid at thermodynamic equilibrium.
2. The gas is incompressible.
3. The plasma flow is laminar and time dependent.
4. The ratio of gas pressure to magnetic pressure is much greater than one.
5. Inductive currents are negligible.

The numerical foundation of the model consists of ten equations. These equations include three fundamental laws of physics (conservation of mass, conservation of energy, and conservation of momentum), the ideal gas law, the enthalpy-temperature relationship for an ideal gas, and a set of Maxwell's equations that assume electrical global neutrality and a simplified Ohm's law approximation [17]. This model serves to simulate arcing phenomena to develop a greater understanding of the underlying physical mechanisms.

2.5 DC Arc-flash Testing

Currently, IEEE 1584-2018 does not provide a method for calculating incident energy for arc-flash in DC systems. The lack of an equation stems from a lack of empirical data. Some research has been conducted to develop empirical arc-flash data for DC systems. Different DC sources have been employed during these testing efforts. For this thesis, attention will be focused on DC arc-flash testing efforts that utilize rectifiers or batteries as sources. Based on research conducted so far, the source will affect arcing

behavior. A rectifier is the most controllable DC source and therefore serves as a baseline compared to the other DC sources. Solar PVs and batteries are more erratic due to their fuel sources (the sun for solar PVs and electrochemical reactions for batteries). Since the research presented in this thesis pertains to battery systems, DC arc-flash testing using solar PVs will be omitted for conciseness. The information presented here is not all inclusive, as additional DC arc-flash tests may have been performed by others without publication of the results.

2.5.1 Kinectrics

The DC arc-flash tests performed by Kinectrics were requested by Bruce Power and presented in a test report titled “DC Arc Hazard Assessment Phase II [18].” These tests produced some of the earliest empirical data for DC arc-flash. The source utilized for testing was a low-voltage AC transformer and a DC bridge rectifier. DC-specific testing established 130 V_{DC} and 260 V_{DC} as the voltage levels. For each voltage level, bolted fault current was employed as an independent variable. Two bolted fault current scenarios were performed for the 130 V_{DC} testing whereas six bolted fault current scenarios were utilized for the 260 V_{DC} testing. The bolted fault currents in the 130 V testing were 4 kA and 20 kA. The bolted fault currents in the 260 V_{DC} testing were 2, 4, 8, 12, 20, and 25 kA. Gap width was a second independent variable used for testing. For both series of tests, gap widths of 0.25, 0.50, 1, and 2 inches were utilized. In addition, Kinectrics performed a series of test to assess the relationship between the heat flux produced by DC arcs and working distance [18].

Kinectrics observed that DC arcs exhibit a trend similar to the Inverse Square Law when assessing the relationship between heat flux and working distance. Deviation from the Inverse Square Law was attributed to “an added heat convection or hot plasma factor at close proximity to the arc [18].” Some findings from the 130 V_{DC} DC tests include a possible threshold of arc sustainability at a 0.5-inch gap width, and that arcs sustained at 0.5-inches can result in incident energy levels that require PPE. The 260 V_{DC} DC tests revealed that, while higher arcing currents occurred at smaller gap widths, greater heat flux was produced at a 1-inch gap width. Furthermore, the 260 V_{DC} test results show that arc sustainability improved with increasing fault current, resulting in greater arc stability and duration. In addition, Kinectrics compared the behavior of DC arcs to similar AC arcs. It was observed that DC arcs were sustainable at lower voltages and produced greater heat flux than their AC counterparts [18].

2.5.2 Bonneville Power Administration

The Bonneville Power Administration (BPA) published research regarding DC arc-flash testing in 2018 [19]. The source used for testing was a 125 V_{DC}, 1,300 Ah capacity battery. Furthermore, the battery type used was flooded lead-acid. The bolted fault current associated with the battery source was 11,000 A. Fifty tests were performed during the testing program. Arcs were initiated inside of a DC panel board that contained two rectangular bus bars. Gap widths employed during testing include 0.25 and 0.50 inches. Some tests were performed at greater gap widths to assess arc sustainability.

Incident energy was measured at an 18-inch working distance throughout testing. Furthermore, BPA performed some tests to assess charger contributions to an arcing fault [19].

BPA observed that there was difficulty in sustaining arcs at a 0.50-inch gap width. Arcs at greater gap widths would self-extinguish rapidly. During testing, the greatest arc duration sustained was 0.715 seconds. In addition, the greatest incident energy measured was 0.9 cal/cm². Results of tests performed with the battery charger connected showed that the charger would contribute approximately 150% of its maximum current rating to the fault, which is consistent with IEEE 946-2004 (*IEEE Recommended Practice for the Design of DC Auxiliary Power Systems for Generating Systems*) [20]. Furthermore, BPA noted that larger gap widths resulted in lower arcing currents; however, arcs typically exhibited current levels close to half of the bolted fault current [19].

2.5.3 American Electric Power

American Electric Power (AEP) pursued DC arc-flash testing in 2018 to assess potential hazards posed by AEP's substation battery backup systems [1]. Two 125 V_{DC} batteries were utilized for testing. One battery had a capacity of 150 Ah and the other battery had a capacity of 100 Ah. The batteries were connected in parallel to increase the fault current since both batteries were retired due to age. The test setup was based on IEEE 1584-2002. One key difference between the test setup used by AEP and IEEE 1584-2002 is the addition of an insulating barrier. Research regarding the IEEE 1584-2002 test setup found that the inclusion of an insulating barrier improves the sustainability of low-voltage arcs and simulates equipment such as terminal blocks [21]. Two independent variables were utilized: gap width and working distance. Gap widths tested ranged from 0.063 (1/16) inches to 0.25 inches. Working distances ranged from six inches to 22 inches. Test duration was standardized at 200 ms to match testing performed for IEEE 1584-2002 [1].

Data analysis focused on two relationships: incident energy vs. working distance and arc energy vs. gap width. A trend similar to the Inverse Square Law was observed when assessing the relationship between incident energy and working distance. As for arc energy and gap width, a parabolic relationship was observed. The parabolic relationship was explained via the maximum power transfer theorem. The two relationships were combined to form an equation to predict incident energy based on gap width and working distance. A linear relationship with time was assumed to modify the equation to account for different arc durations. The equation developed is represented by (11) [1].

$$IE = \frac{0.05263(-28,730(GW^2) + 11,230(GW) + 5061)t}{WD^{2.172}} \quad (11)$$

where:

IE = incident energy (cal/cm²)

GW = gap width (in)

WD = working distance (in)

t = arc duration (s)

Equation (11) was compared with the Doan Model and the Ammerman Model. Behavior was similar among the three models with the open-air version of the Ammerman Model exhibiting the closest behavior to (11). Since there was similar behavior among the three models, the empirical model served to confirm the validity of the Doan Model and the Ammerman Model [1].

2.5.4 Hydro-Quebec

Hydro-Quebec recently had a series of DC arc-flash tests performed at a high-voltage lab in Toronto, Ontario, CA. The results of the tests were published in 2020 as part of the Electrical Safety Workshop in the paper titled “Low Voltage 100-500 Vdc Arc Flash Testing” by Kirk Gray, S. Robert, and Timothy L. Gauthier [22]. Hydro-Quebec has a wide range of DC voltage levels present in their system; therefore, testing included a voltage range of 100 V_{DC} to 520 V_{DC}. In addition, bolted fault current levels ranged from seven kA to 20 kA. The test setup was based on IEC 61482-1-2 (*Live Working – Protective Clothing against the Thermal Hazards of an Electric Arc – Part 1-2: Test Methods – Method 2: Determination of Arc Protection Class of Material and Clothing by using a Constrained and Directed Arc (Box Test)*). Therefore, electrodes were placed vertically in series (end-to-end) instead of vertically in parallel as shown in IEEE 1584. Furthermore, some tests were performed with an enclosure while others were performed without an enclosure. There were 23 tests performed with three replications each to account for arc variability [22].

As would be expected, arc duration increased with increased voltage levels. Tests were limited to a two-second duration. No arcs could be sustained the full two seconds until the 500 V source was employed. Incident energy emitted during these full duration tests peaked at 44 cal/cm². In addition, the test results were compared with incident energy predictions generated by DC arc-flash software. For 105 V_{DC} to 144 V_{DC}, the DC arc-flash software overestimated the incident energy to varying degrees using a 25 mm gap width. At 260 V_{DC} and 520 V_{DC}, the DC arc-flash software underestimated incident energy at 25 mm gap width. Using the average gap width instead of the 25 mm gap width brought predicted incident energy levels within range of the measured values. Besides DC arc-flash software, test results were compared with the predicted incident energy calculated via the Maximum Power Method (similar to the Doan Method and Lee Method depicted in IEEE 1584). The Maximum Power Method overestimated incident energy for all voltage levels. Arc sustainability was difficult at 105 V_{DC} and no test produced incident energies greater than 1.2 cal/cm² at that voltage level. A voltage level of 140 V_{DC} resulted in incident energy measurements greater than 1.2 cal/cm². Lastly, arcs were not sustainable at voltage levels less than 100 V_{DC} [22].

2.6 Chapter Summary

Arc-flash is a complicated area of research with a long history of interest by numerous organizations resulting in a variety of publications, models, standards, and guidelines. The following are some high-level ideas addressed by this chapter:

- Arc-flash is a serious hazard posed by electrical systems that can cause harm via heat, pressure, light, and sound.
- To mitigate the risk of arc-flash hazards, studies are performed to quantify incident energy (a measure of thermal energy) to develop countermeasures.
- Guidance for incident energy calculations is contained in IEEE 1584. PPE and other safety measures are defined by NFPA 70E. It should be noted that IEEE 1584 does not address DC arc-flash hazards due to a lack of empirical data.
- Researchers have proposed various theoretical and semi-empirical models to address DC arc-flash hazards.
- Some research has been dedicated to the empirical testing of DC arc-flash to develop a greater understanding and generate the data necessary to define an empirical equation for DC arc-flash similar to those developed for AC arc-flash.
- Trends in the electrical utility industry are leading to the proliferation of multiple sources of DC electricity. These different sources result in variations in arcing behavior thereby complicating the development of empirical DC arc-flash equations.

CHAPTER 3: METHODOLOGY

3.1 Testing Arrangement and Equipment

The testing presented in this thesis is a continuation of a series of tests conducted in August 2018 [1], [2]. Therefore, the test arrangement and equipment are similar to the previous tests [2]. Two 125 V_{DC} batteries were utilized for testing. A third 125 V_{DC} battery (the 100 Ah battery from the August 2018 tests) was planned to be used; however, the battery had deteriorated beyond usability. One battery was used in the first test series and had a capacity of 150 Ah. The second battery was acquired for this additional series of tests. The acquired battery had a capacity of 400 Ah. Some tests were conducted with only the 400 Ah batteries whereas other tests used the two batteries connected in parallel.

Arcs were initiated in a 20-inch by 20-inch by 20-inch enclosure was used to simulate the concentration effect of incident energy for equipment contained in enclosures. Electrodes were inserted through the roof of the enclosure, four inches from the back panel. An insulating board was included at the tips of the electrodes due to benefits to low-voltage arc stability and similarity to equipment [21], such as terminal blocks, which are commonly contained in panel boards. The circuit connecting the battery sources and the enclosure included a series of disconnect switches, a pair of battery chargers, and a DC circuit breaker. The disconnect switches managed connections between the batteries and the enclosure and provided visual assurance that the circuit was de-energized prior to performing any work on the circuit. The battery chargers served to maintain the energy levels of the batteries. They were not connected during testing. Lastly, the DC circuit breaker was used to both manage the test duration as well as provide an additional means to de-energize the test circuit in case of emergency. A power schematic of the testing arrangement is depicted in Figure 3.1 [23].

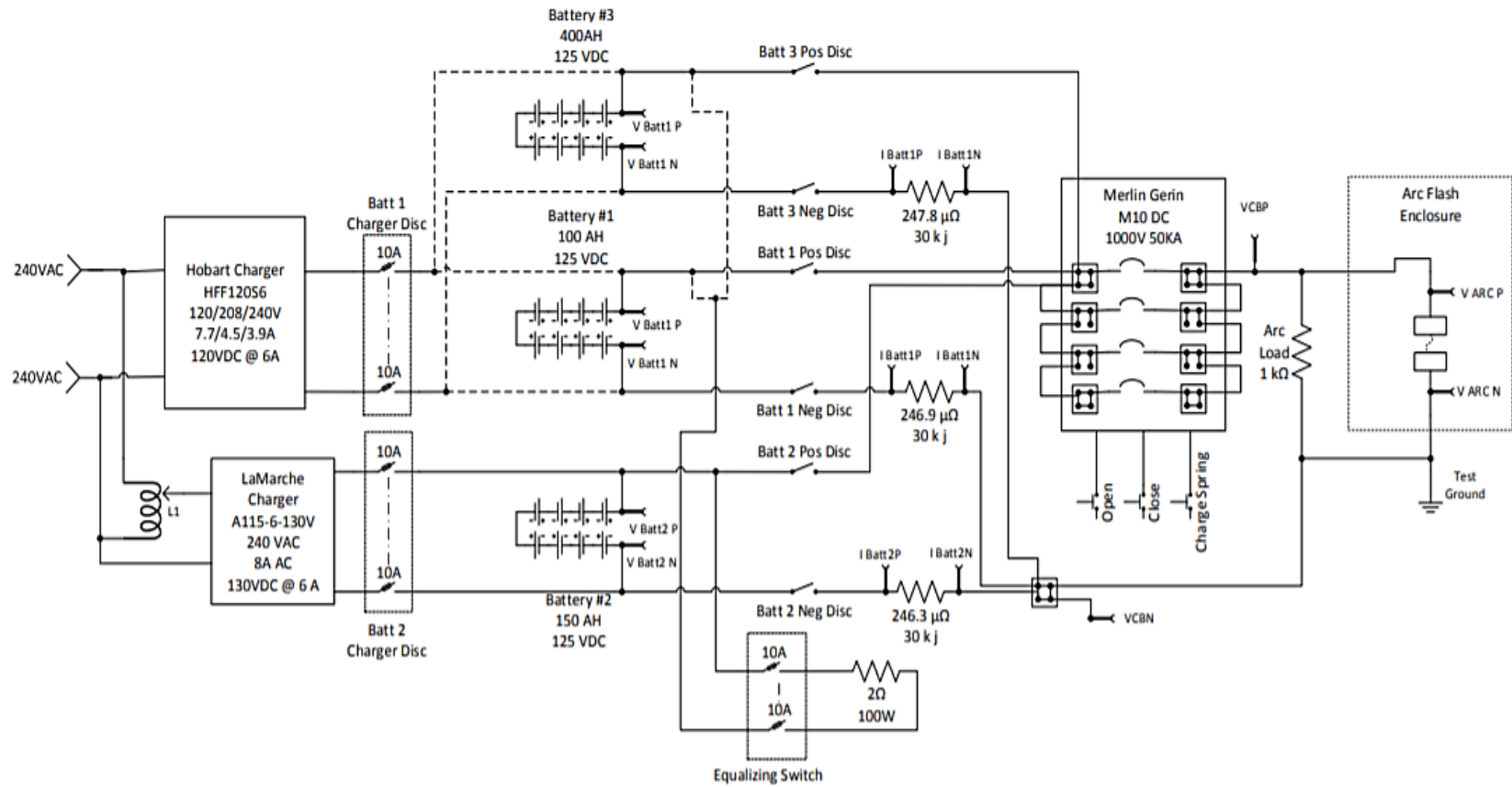


Figure 3.1: Power Schematic of Testing Arrangement [23]

The largest change between the August 2018 tests and the February 2019 tests was location. Originally, testing was performed in the outside environment. Since atmospheric conditions were speculated to have affected arc sustainability on August 8th, the test arrangement was moved indoors [2]. Furthermore, atmospheric conditions (specifically temperature and relative humidity) were added as test variables. To control temperature and humidity, the enclosure was placed inside an environmental chamber. The environmental chamber had temperature control and precipitation capabilities. Since the environmental chamber could only add moisture by default, an industrial dehumidifier was connected to the environmental chamber to enable the removal of moisture. This allowed greater control of the environment within the chamber. The test enclosure inside the environmental chamber is depicted in Figure 3.2 [23]. The temperature and humidity controls for the chamber are displayed in Figure 3.3 [23].



Figure 3.2: Test Enclosure in Environmental Chamber [23]



Figure 3.3: Environmental Chamber and Dehumidifier Controls [23]

Thermal measurements and video recordings were captured for each test. Calorimeters were made in accordance with IEEE 1584. A stand was constructed to hold the calorimeters. The calorimeter arrangement utilized for testing was a 2-3-2 pattern. Type K thermocouples were used to attach the calorimeters to the data acquisition module. Video recordings were made using standard and slow-motion cameras. Performing tests within the environmental chamber presented some difficulty with lighting. Standing lights were used to help visibility in the environmental chamber. A summary of all test and measurement equipment is included in Table 3.1.

Table 3.1: Summary of Testing Equipment

Description	Manufacturer	Model
Data Acquisition Systems (DASs)		
Main DAS	Genesis	---
Thermal Couple DAS	HBM	Quantum MX809B
DAS Chassis	HBM	LD-645-1000663
Video Recorders		
Standard Speed Camera	GoPro	Hero 7
High Speed Camera	NAC	MemRecam GX-3, Model V-190
Battery Chargers		
Battery Charger 1	Hobart	HFF120S6
Battery Charger 2	LaMarche	A112-6-130V
Batteries		
Battery 1	BAE	12 V 4 OGi 100-N6 LA
Battery 2	Power Safe-C	3CA-7
Battery 3	BAE	5 OGi 400 LA
Other Test Arrangement Equipment		
DC Circuit Breaker	---	---
Type K Thermocouple	Omega	5TC-GG-K-30-36
Environmental Chamber	Webber	---
Dehumidifier	Alorair	Storm Elite

3.2 Test Setups

Prior to starting the tests, a number of desired test setups were developed. During the creation of these test setups, attention was paid to the amount of time required to complete testing. Therefore, the setups were developed to minimize the amount of testing required while providing a strong understanding of DC arc-flash behavior. Furthermore, test setups were arranged to minimize downtime between tests. The test setups are summarized in Table 3.2.

Table 3.2: DC Arc-flash Stage 2 Test Setups - Planned

Setup Parameters						
Test Setup	Batteries Used	Temp. (°F)	Rel. Humidity (%)	Gap (in.)	Distance (in.)	Duration (sec.)
1	100+150	68	20	0.0625	15	0.2
2	100+150	68	20	0.125	15	0.2
3	100+150	68	20	0.250	15	0.2
4	100+150	68	20	0.500	15	0.2
5	400+150	68	20	0.0625	15	0.2
6	400+150	68	20	0.125	15	0.2
7	400+150	68	20	0.250	15	0.2
8	400+150	68	20	0.500	15	0.2
9	400+150	68	20	Max Energy	15	2
10	400+150	85	20	Max Energy	15	2
11	400+150	32	20	Max Energy	15	2
12	400+150	32	80	Max Energy	15	2
13	400+150	68	80	Max Energy	15	2
14	400+150	85	80	Max Energy	15	2
15	400+150	85	40	Max Energy	15	2
16	400+150	68	40	Max Energy	15	2
17	400+150	32	40	Max Energy	15	2
18	400+150	68	20	0.125	12	0.2
19	400+150	68	20	0.125	9	0.2
20	400+150	68	20	0.125	6	0.2

After attempting the first test setup, it was discovered that Battery 1 had deteriorated since the conclusion of the first stage of testing. Therefore, the test setups requiring Battery 1 were skipped and testing proceeded using Battery 2 and 3 in parallel. After completing all other planned tests, attempts were made to revive Battery 1. The first attempt sought to charge the battery to a sufficient voltage level to “clean” the electrodes. There was no appreciable change in battery performance as a result. Since “cleaning” the electrodes was unsuccessful, the next course of action was to attempt to identify any bad cells in the battery string and remove them. The plan to identify bad cells was to attach voltage probes at various points in the battery string to create groups of cells. A group showing signs of a bad cell would be subdivided into smaller groups using voltage probes. This procedure would be repeated until all bad cells were identified. It became clear after a couple attempts that identifying the bad cells would be no simple task as negative voltages were encountered, indicating that currents were flowing in reverse directions at different points of Battery 1. It was decided that Battery 1 was unsalvageable.

Since Battery 1 could not be salvaged, the test plan was revised accordingly. During testing, it was noted that Battery 3 could supply fault current levels similar to Battery 1 and 2 connected in parallel (test setup 1-4). Therefore, those test setups were revised to use Battery 3 alone. Furthermore, some additional tests were performed to assess the arc durations possible with Battery 3. Thus, 23 test setups were utilized in the testing program. These test setups are summarized in Table 3.3. Based on the testing procedure established during the 2018 DC arc-flash testing, most test setups were performed three times to account for the variability of arcs with retests being performed as required. Therefore, approximately 80 tests were performed during the testing period, which began February 18th and ended March 1st.

Table 3.3: DC Arc-flash Stage 2 Test Setups - Revised

Setup Parameters						
Test Setup	Batteries Used	Temp. (°F)	Rel. Humidity (%)	Gap (in.)	Distance (in.)	Duration (sec.)
1	400	68	20	0.0625	15	0.2
2	400	68	20	0.125	15	0.2
3	400	68	20	0.250	15	0.2
4	400	68	20	0.500	15	0.2
5	400+150	68	20	0.0625	15	0.2
6	400+150	68	20	0.125	15	0.2
7	400+150	68	20	0.250	15	0.2
8	400+150	68	20	0.500	15	0.2
9	400+150	68	20	Max Energy	15	2
10	400+150	85	20	Max Energy	15	2
11	400+150	32	20	Max Energy	15	2
12	400+150	32	80	Max Energy	15	2
13	400+150	68	80	Max Energy	15	2
14	400+150	85	80	Max Energy	15	2
15	400+150	85	40	Max Energy	15	2
16	400+150	68	40	Max Energy	15	2
17	400+150	32	40	Max Energy	15	2
18	400+150	68	20	0.125	12	0.2
19	400+150	68	20	0.125	9	0.2
20	400+150	68	20	0.125	6	0.2
21	400	68	20	0.125	15	2
22	400	68	20	0.250	15	2
23	400	68	20	0.500	15	2

3.3 Testing Procedure

Test duration was varied based on the relationship being assessed. For tests focused on gap width and working distance, the test duration was typically standardized

at 200 ms, similar to IEEE 1584. Test setups 21, 22, and 23 deviate from the 200 ms standard to assess the greatest arc duration possible with the 400 Ah battery. Test setups 9 through 17 were standardized at two seconds since arc duration was the parameter of interest when manipulating temperature and relative humidity. Prior to each test, the batteries were charged slightly above 125 V_{DC} (approximately 130 V_{DC} to 133 V_{DC}). Afterwards, the batteries were disconnected from the chargers and connected to the test circuit. During this operation, the DC circuit breaker was open for safety. After the switching operation was complete, a remote control was used to close the breaker to initiate the arc. A 20 AWG fuse wire wrapped in a figure-8 was used to create the short between the copper electrodes. The fuse wire would rapidly vaporize after the breaker closed and establish an arc. Once the arc extinguished, the batteries were disconnected from the test circuit and reconnected to the chargers to replenish energy.

This general procedure was followed for every test. For tests focused on atmospheric conditions, there was additional downtime to allow the environmental chamber to meet the desired temperature and relative humidity levels. Note that temperature and relative humidity levels were approximate for all tests due to control difficulty. Downtime between tests also increased as test duration increased due to the increased energy expended by the batteries.

Each test setup was repeated a total of at least three replications. Some test setups were repeated additional times if unexpected or poor arcing behavior occurred. Performing multiple replications of the test setups was pursued to account for arc variance. After each test, while the batteries recharged, the test arrangement was reset. Electrodes were removed and refinished. Multiple electrode ends were prepared to minimize downtime. Occasionally, the insulating barrier would be replaced if deterioration was extensive. A summary of the testing procedure is contained in

Table 3.4. Test Setups 1 through 8 and Test Setups 21 through 23 are classified as “Gap Width Tests” due to gap width being the independent variable during those test setups. Test Setups 9 through 17 are considered “Atmospheric Condition Tests” because relative humidity and environmental temperature were the independent variables for those test setups. Lastly, Test Setups 18 through 20 are termed “Working Distance Tests” since working distance served as the independent variable.

Table 3.4: Summary of Testing Procedure

General Testing Procedure for Gap Width Tests	
Step 1:	Set electrodes to desired gap width
Step 2:	Perform switching operation to connect enclosure to battery circuit
Step 3:	Initiate test via DC circuit breaker controls
Step 4:	Terminate test via DC circuit breaker after 200 ms or two seconds as appropriate
Step 5:	Perform switching operation to disconnect enclosure from battery circuit
Step 6:	Record results and reset electrodes in enclosure
Step 7:	Repeat Steps 2 – 6 at least two times (or until three full duration tests are performed)
Step 8:	Select new gap width and repeat Steps 1 – 7 until all test setups are complete
General Testing Procedure for Working Distance Tests	
Step 1:	Set electrodes to 0.125-inch gap width
Step 2:	Move calorimeter stand to desired distance from electrodes
Step 3:	Perform switching operation to connect enclosure to battery circuit
Step 4:	Initiate test via DC circuit breaker controls
Step 5:	Terminate test via DC circuit breaker after 200 ms
Step 6:	Perform switching operation to disconnect enclosure from battery circuit
Step 7:	Record results and reset electrodes in enclosure
Step 8:	Repeat Steps 3 – 7 at least two times (or until three full duration tests are performed)
Step 9:	Select new working distance and repeat Steps 2 – 8 until all test setups are complete
General Testing Procedure for Atmospheric Condition Tests	
Step 1:	Set electrodes to gap width with greatest incident energy
Step 2:	Set environmental chamber to desired configuration
Step 3:	Monitor environmental chamber until appropriate temperature and humidity levels are achieved
Step 4:	Perform switching operation to connect enclosure to battery circuit
Step 5:	Initiate test via DC circuit breaker controls
Step 6:	Terminate test via DC circuit breaker after two seconds
Step 7:	Perform switching operation to disconnect enclosure from battery circuit
Step 8:	Record results and reset electrodes in enclosure
Step 9:	Repeat Steps 3 – 8 at least two times
Step 10:	Select new environmental chamber configuration and repeat Steps 2 – 10 until all test setups are complete

CHAPTER 4: DATA ANALYSIS

4.1 Gap Width Analysis

4.1.1 Relationship between Gap Width and Maximum Temperature Rise

Gap width and maximum temperature rise exhibits a polynomial trend as determined by a curve fit analysis performed in Microsoft Excel. Though a trend exists, there is a significant amount of spread among the various values, making it difficult to be certain of how reliable this relationship is. A more rigorous statistical analysis may reveal whether or not the relationship is significant and allow for determination of the error associated with each measurement, which would provide a means to assess the model's appropriateness. The relationship along with its corresponding equation is depicted in Figure 4.1. It should be noted that the relationship displayed is the same as the relationship between gap width and peak incident energy. This is due to incident energy and calorimeter temperature rise being related by a constant of $0.135 \text{ cal}/((\text{cm}^2)(^\circ\text{C}))$. In addition, the trend showed some consistency among the different battery configurations. The relationship associated with Battery 3 being used independently is depicted in Figure 4.2.

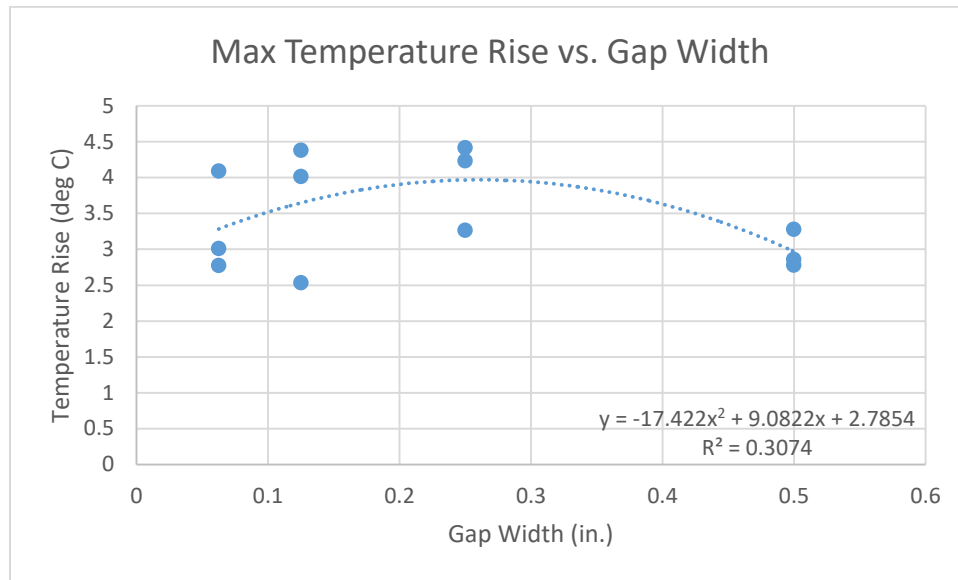


Figure 4.1: Gap Width and Max Temperature Rise Relationship for Battery 2 & 3

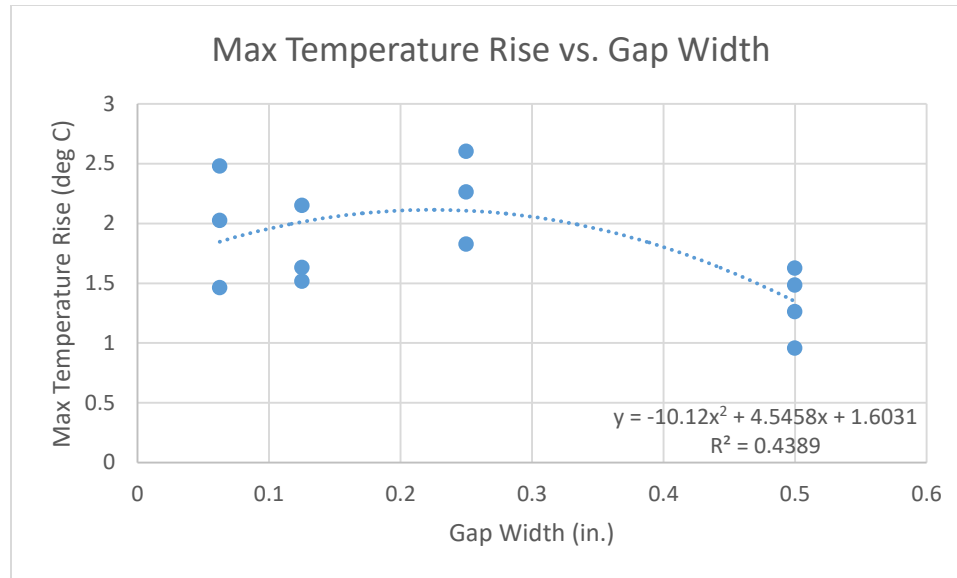


Figure 4.2: Gap Width and Max Temperature Rise Relationship for Battery 3

4.1.2 Relationship between Gap Width and Arc Characteristics

The influence of gap width on a variety of arc characteristics was analyzed. The arc characteristics included were current, voltage, resistance, and energy. For current, voltage, and resistance, the values used were taken from the point in time that the arc was generated and the fuse wire was vaporized. The reason for selecting a specific point in time to acquire values is for simplification. During each test, arc voltage and current fluctuated due to the changing environment in which the arc existed. The biggest environmental change was with respect to the electrodes. As the electrodes were consumed by the arc, arc voltage and current changed due to the increasing “gap width” associated with the removal of electrode material. Calculation of arc power in MATLAB utilizing arc voltage and current revealed that, for several arcs, there was a decrease in power as the test proceeded. However, other tests exhibited an increase in arc power over the test duration. Furthermore, some tests exhibited parabolic behavior with a maximum occurring at some point over the power profile. These behaviors are displayed in Figure 4.3, Figure 4.4, and Figure 4.5.

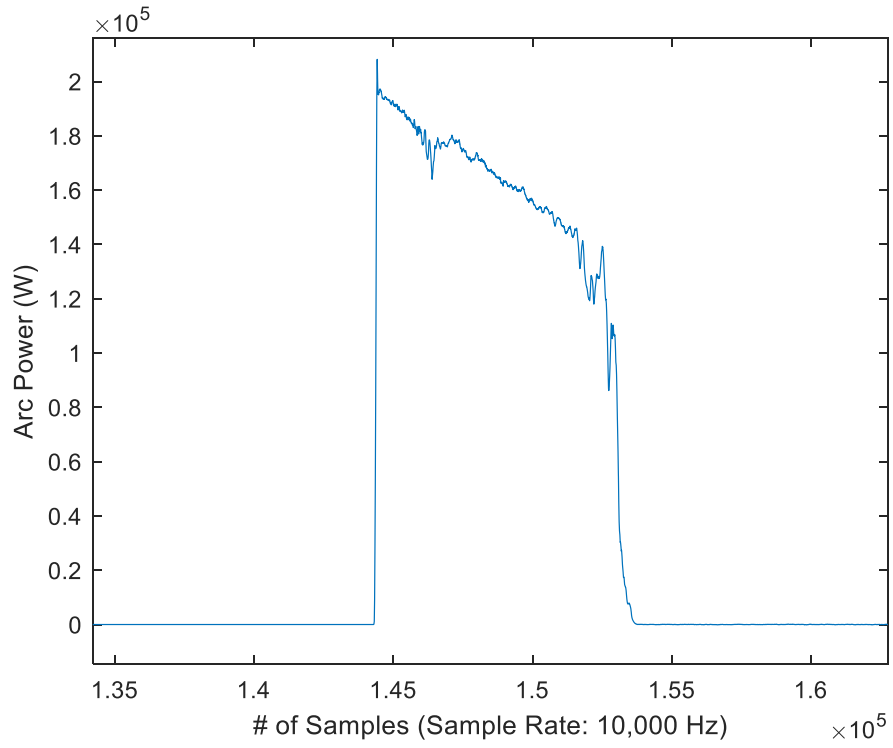


Figure 4.3: Example of Decreasing Arc Power (Power 250R26(9))

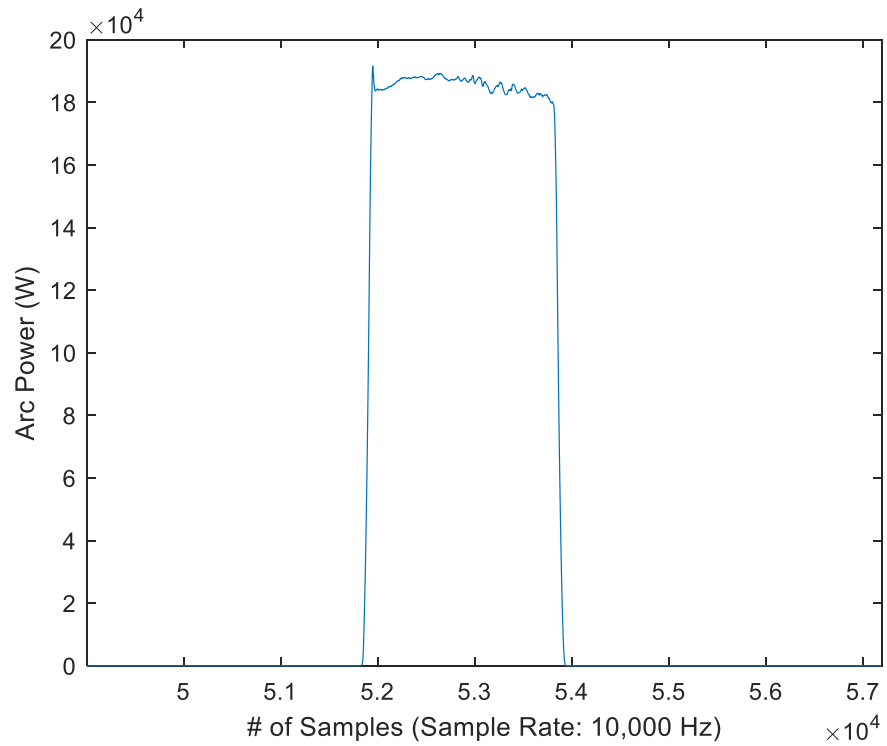


Figure 4.4: Example of Parabolic Arc Power (Power 125R4(5))

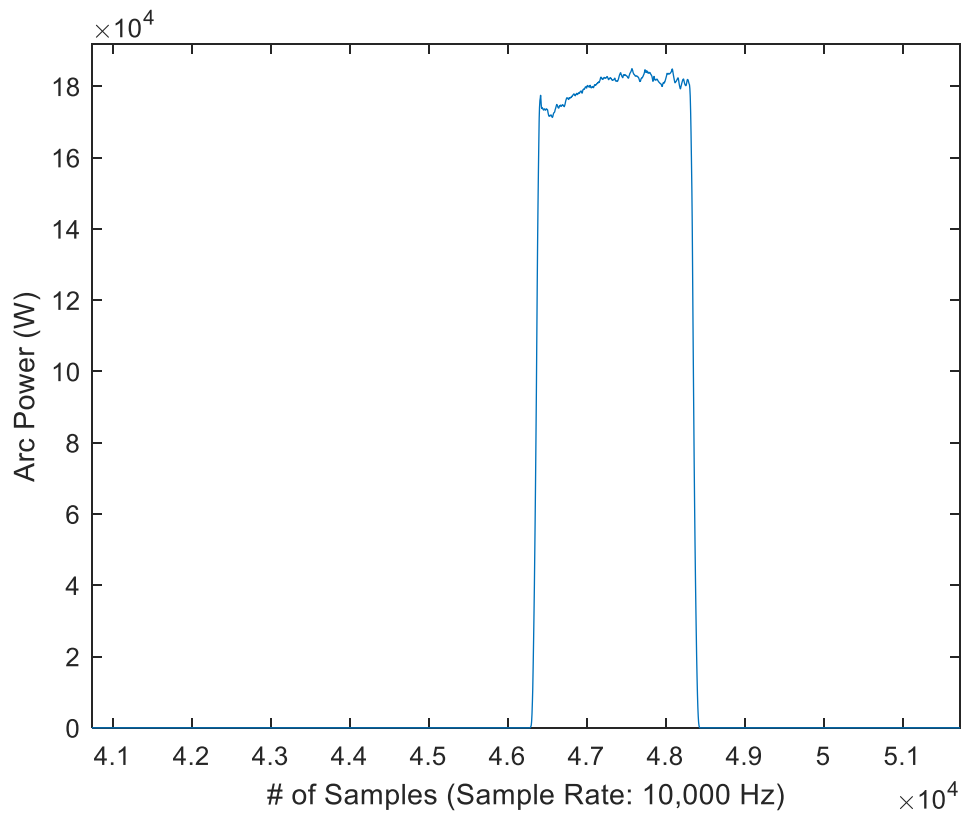


Figure 4.5: Example of Increasing Arc Power (Power 062R26(1))

The relationships between gap width and (1) arc current, (2) voltage, and (3) resistance are displayed in the following figures. Figure 4.6 and Figure 4.7 depict the relationships between gap width and initial arc current. Figure 4.8 and Figure 4.9 display the relationships between gap width and initial arc voltage. Lastly, Figure 4.10 and Figure 4.11 present the relationships between gap width and initial arc resistance. Out of these three, the relationship between gap width and arc resistance is perhaps the most important. Both Figure 4.10 and Figure 4.11 display a positive correlation between gap width and arc resistance. This relationship can be explained by the increased presence of air between the electrodes as gap width increased. Air is a dielectric material and is therefore a poor conductor. Thus, increasing the amount of air between the electrodes increased the amount of resistance the arc had to overcome to bridge the gap.

Arc resistance relates arc voltage and current to each other via Ohm's Law. Gap width shows a positive relationship with arc voltage and a negative relationship with current as expected. In order for the arc to bridge the gap between the electrodes, there must be sufficient energy. Therefore, it can be reasoned that arc voltage (as a form of potential energy) must increase to allow the arc to cross the gap. Current, on the other hand, decreases due to the increased resistance encountered. Power transfer theory can also explain the various arc relationships with gap width. Indicated by the changing arc

behaviors during testing, power transfer states that the amount of power delivered to the load is based on the relationship between the source and load impedances. As the impedance of the load approaches that of the source, the amount of power delivered to the load increases until reaching a maximum. This peak occurs when the source and load impedances are equivalent. The maximum power transfer theorem is based upon this phenomenon. As the load impedance surpasses the source impedance, the magnitude of power across the load impedance gradually diminishes. It is possible that, by increasing the gap width, the resistance of the arc was approaching the impedance of the source. This would also explain the upward trend by arc voltage since the power transferred would be increasing and one definition of electric power is the product of voltage and current.

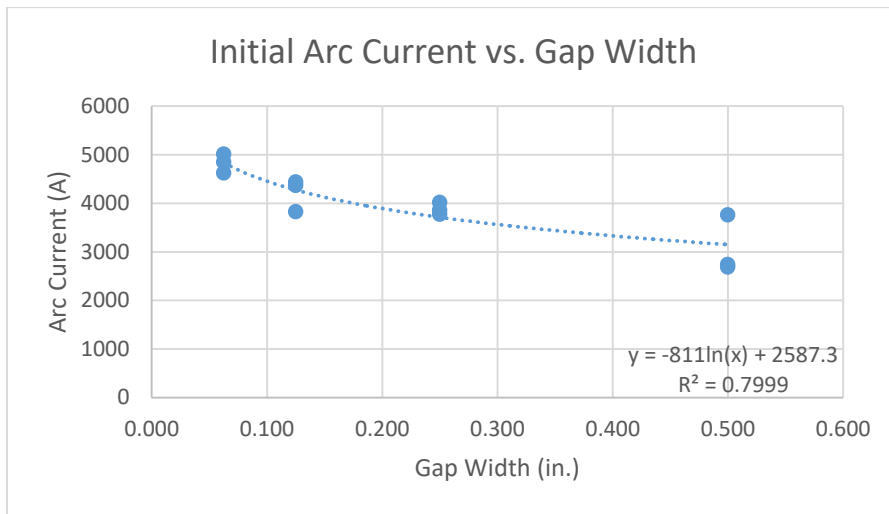


Figure 4.6: Initial Arc Current vs. Gap Width for Batteries 2 & 3

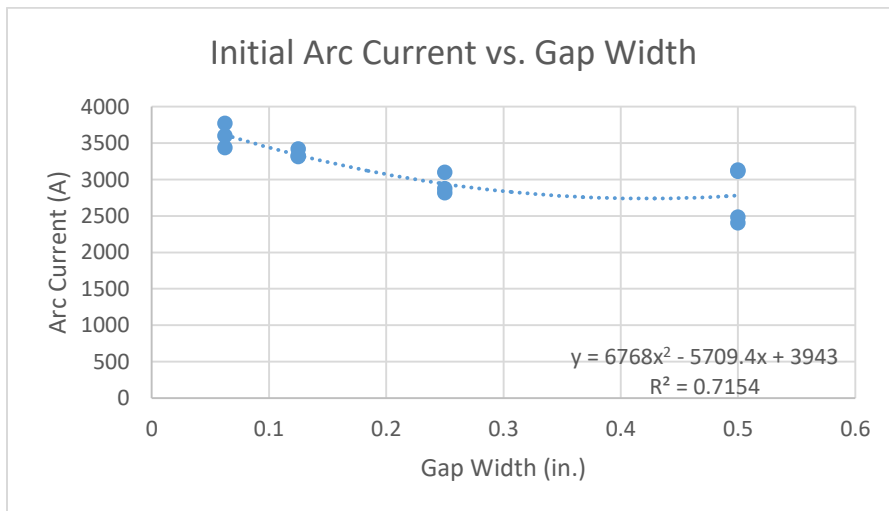


Figure 4.7: Initial Arc Current vs. Gap Width for Battery 3

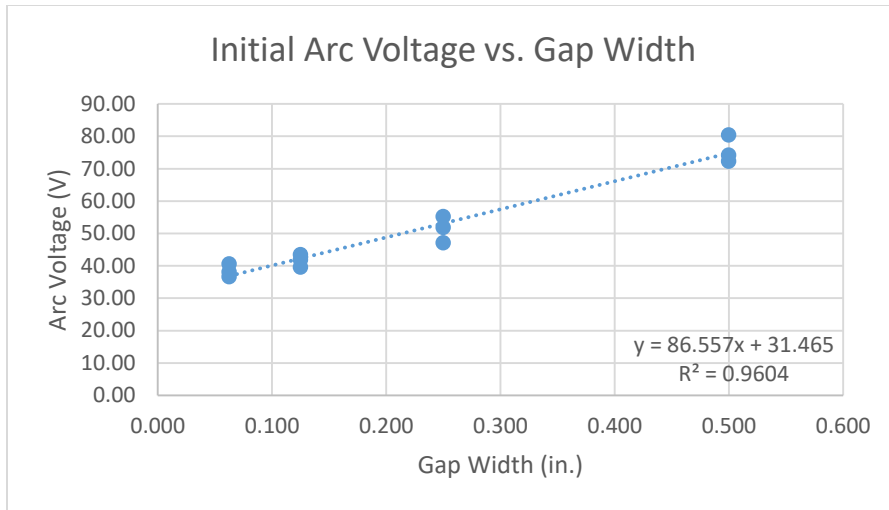


Figure 4.8: Initial Arc Voltage vs. Gap Width for Batteries 2 & 3

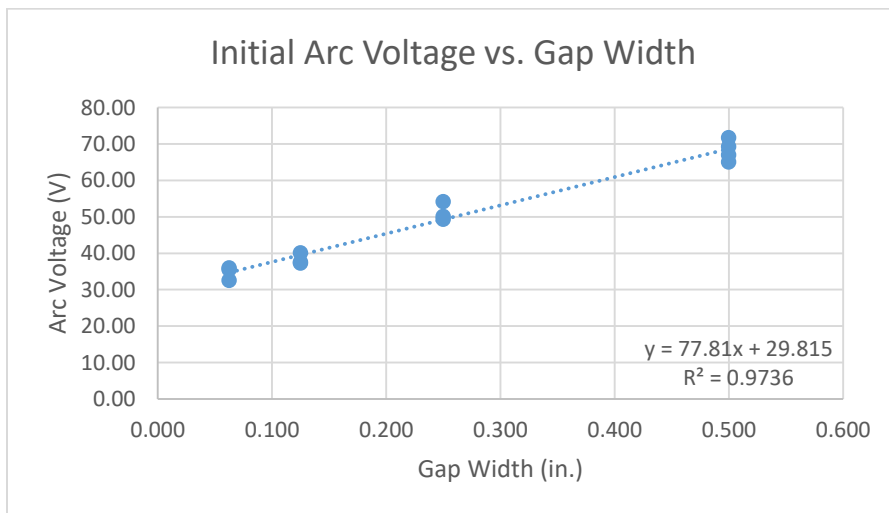


Figure 4.9: Initial Arc Voltage vs. Gap Width for Battery 3

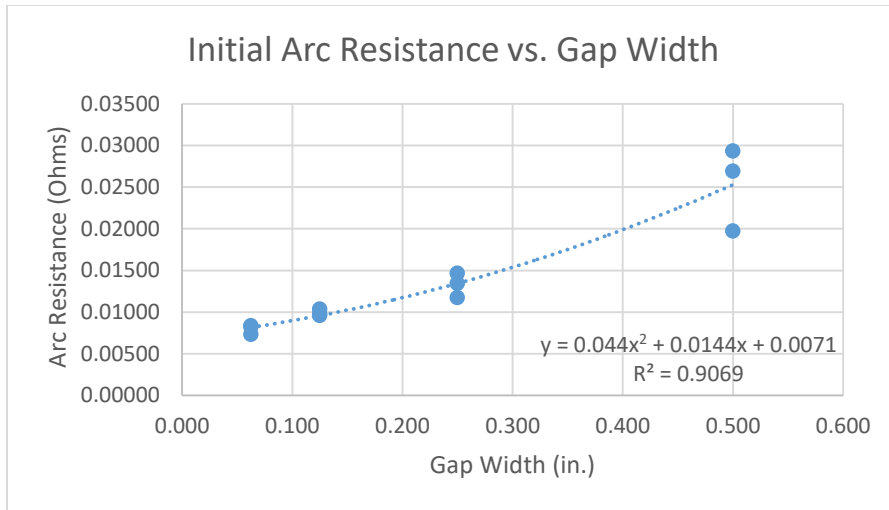


Figure 4.10: Initial Arc Resistance vs. Gap Width for Batteries 2 & 3

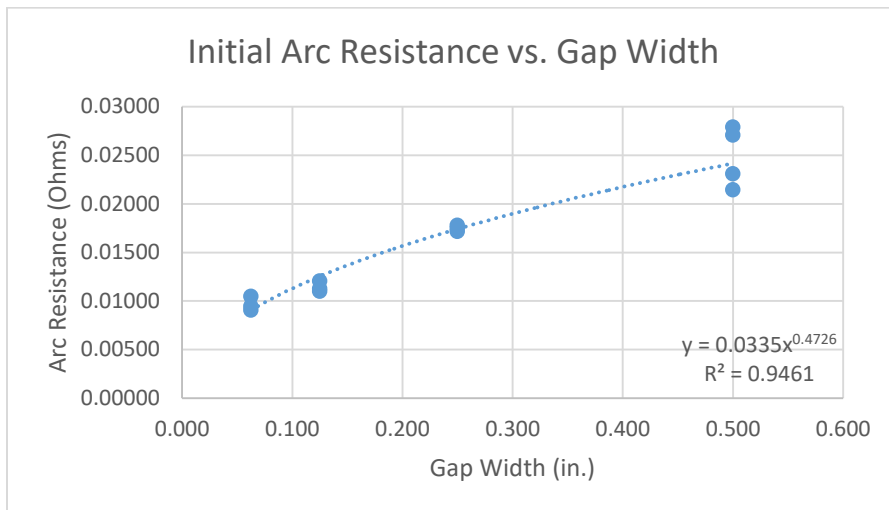


Figure 4.11: Initial Arc Resistance vs. Gap Width for Battery 3

4.1.3 Relationship between Gap Width and Arc Energy

Arc energy was calculated by multiplying the arc currents and voltages for each test and integrating over the duration of the test. The values for arc current and voltage were smoothed using a moving filter with a window size of 10.1 milliseconds. Smoothing the data did result in a lower amount of energy being calculated; however, the difference between using original data versus smoothed data was approximately 1%. Therefore, the loss of accuracy is negligible. Furthermore, the smooth data provides a cleaner depiction of arc behavior over time compared with the original data. This difference in visualization is presented in Figure 4.12.

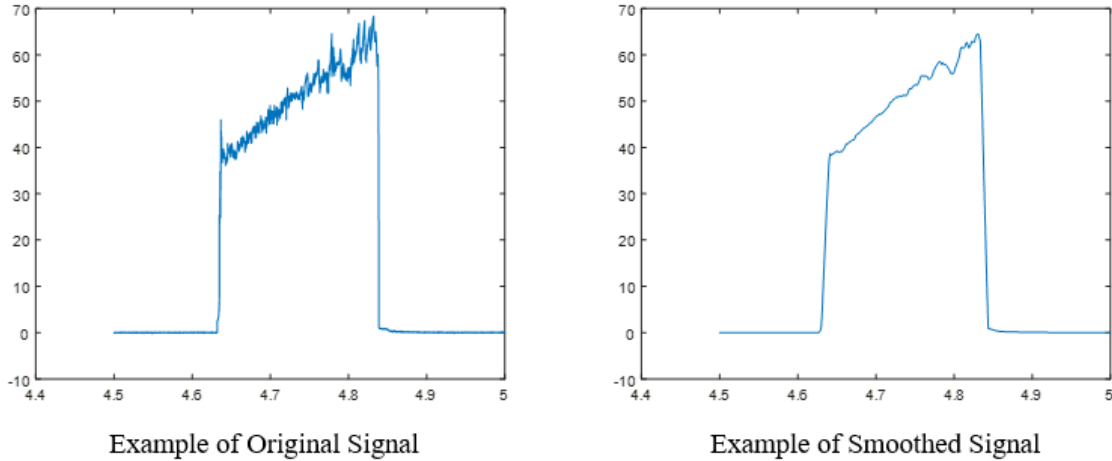


Figure 4.12: Comparison of Original and Smoothed Signals

Gap width displayed two different relationships with arc energy. The first relationship is depicted in Figure 4.13 and is associated with the utilization of Battery 2 and 3. The second relationship is depicted in Figure 4.14 and is associated with the utilization of only Battery 3. During the 2018 testing, a parabolic relationship similar to Figure 4.14 was observed for the relationship between gap width and arc energy. At that time, it was believed that the parabolic relationship was due to power transfer [1], [2].

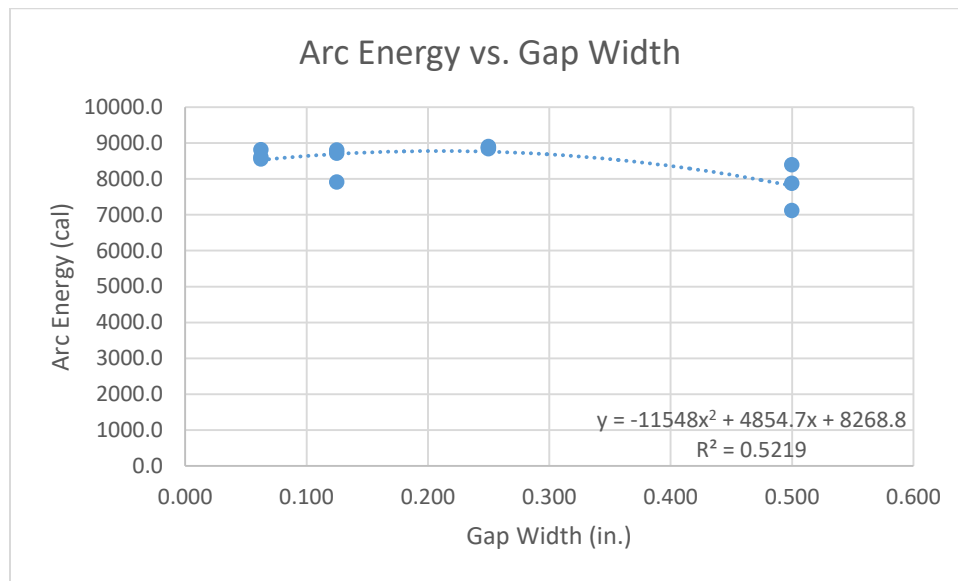


Figure 4.13: Arc Energy vs. Gap Width for Batteries 2 & 3

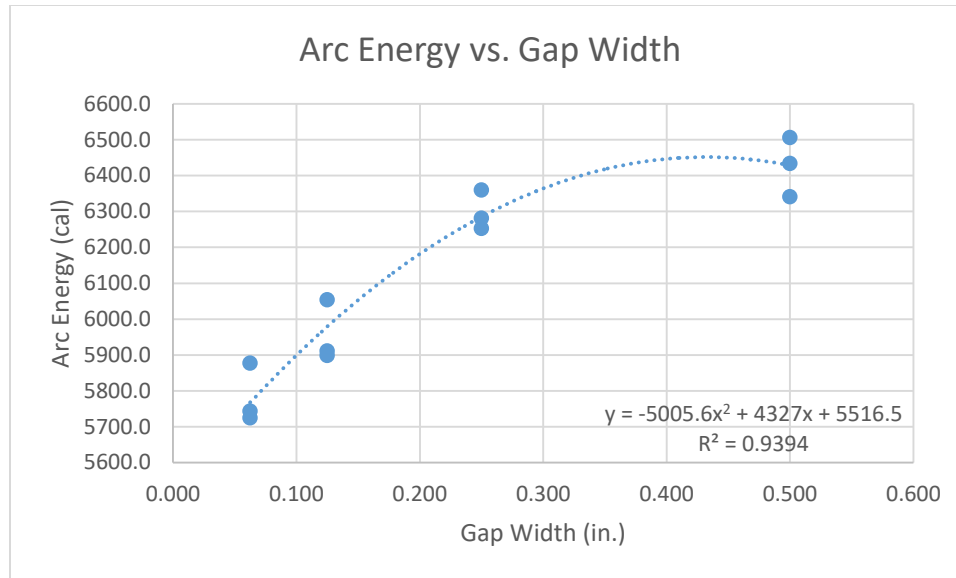


Figure 4.14: Arc Energy vs. Gap Width for Battery 3

Investigation into the gap width-arc energy relationships began with revisiting the maximum power transfer theorem. Figure 4.15 is an example of the trend associated power transfer. This example was constructed using the simple electrical circuit depicted in Figure 4.16. Inspection of Figure 4.15 shows the existence of two different trends. The first trend is to the left of the maximum and mirrors that of a parabola. The second trend is to the right of the maximum and displays a slow decay. Since the graph shows two trends, it was reasoned that both of the relationships in Figure 4.13 and Figure 4.14 might be contained by Figure 4.15 in some capacity. Thus, Figure 4.15 was broken down to search for similarities with Figure 4.13 and Figure 4.14. This search ultimately produced Figure 4.17 and Figure 4.18, which mirror Figure 4.14 and Figure 4.13, respectively. Some deviation is noticeable; however, the overall shape seems to be present. Thus, the maximum power transfer theorem holds as an explanation of the relationships displayed in Figure 4.13 and Figure 4.14. The different relationships are the result of different starting points along the graph depicted in Figure 4.15. The reason behind the different starting points likely stems from the battery configuration. In Figure 4.15, the x-axis is defined by the ratio between load resistance and source resistance. Movement along the x-axis can therefore be achieved one of two ways: increase the load resistance or reduce the source resistance. Based on observation of Figure 4.10 and Figure 4.11 in the previous section, arc resistance (or the load resistance) is consistent among the two battery configurations. Since it does not appear that there is a significant difference in the load resistance, source resistance must have changed to produce the different relationships. The reason battery configuration was identified as the most probable factor in changing the source resistance is due to equivalent impedance decreasing when the batteries are connected in parallel.

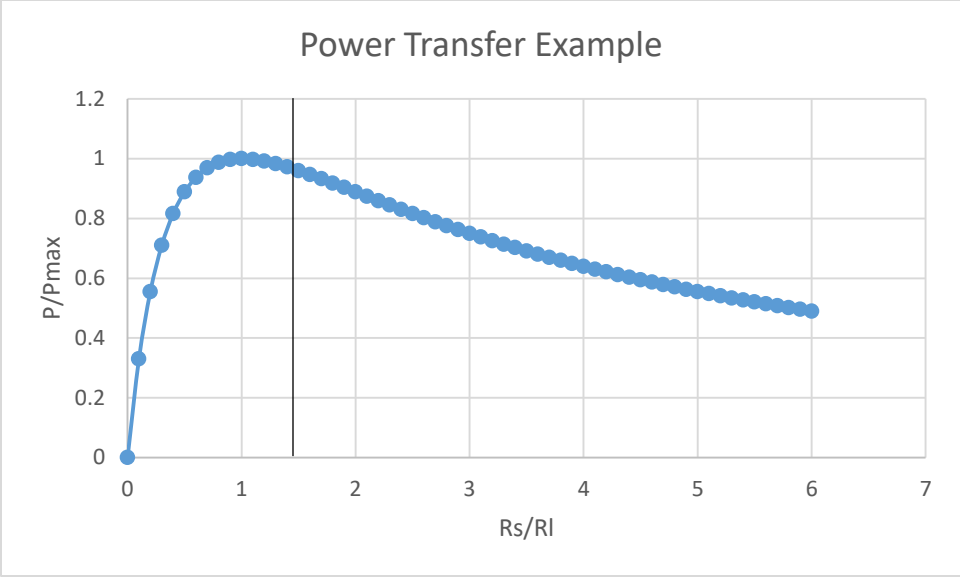


Figure 4.15: Example of Typical Power Transfer Curve

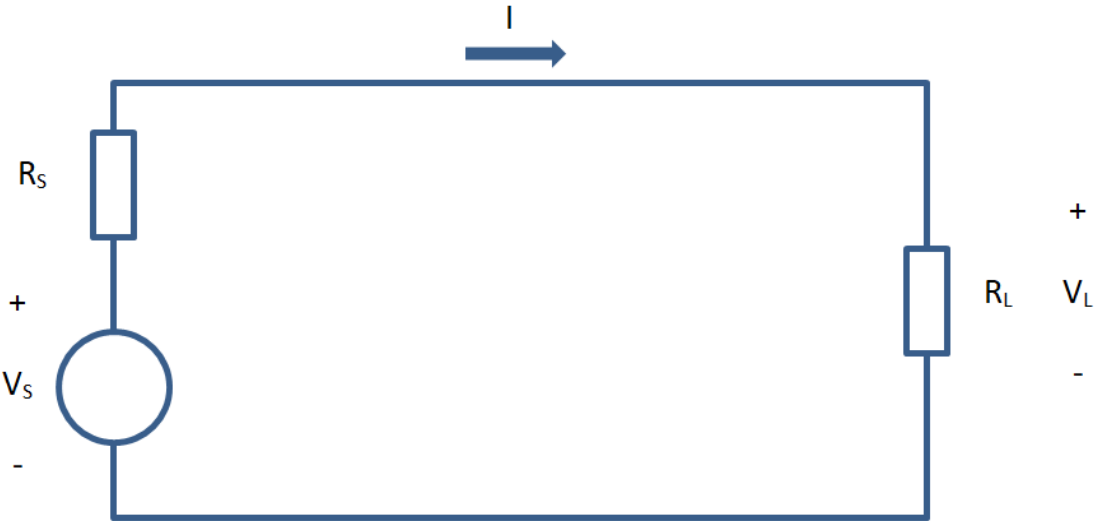


Figure 4.16: Simple Circuit for Power Transfer Example

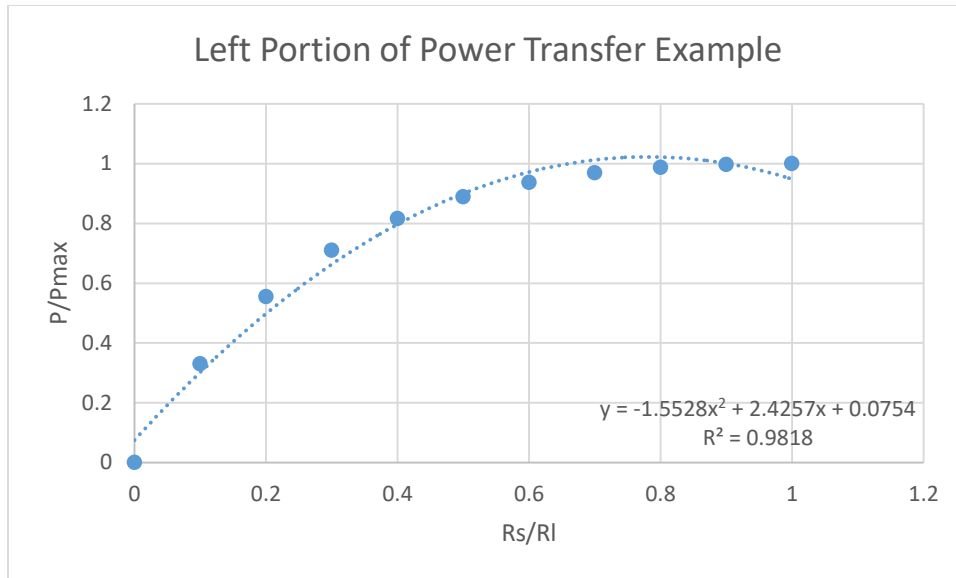


Figure 4.17: Left Portion of Power Transfer Example

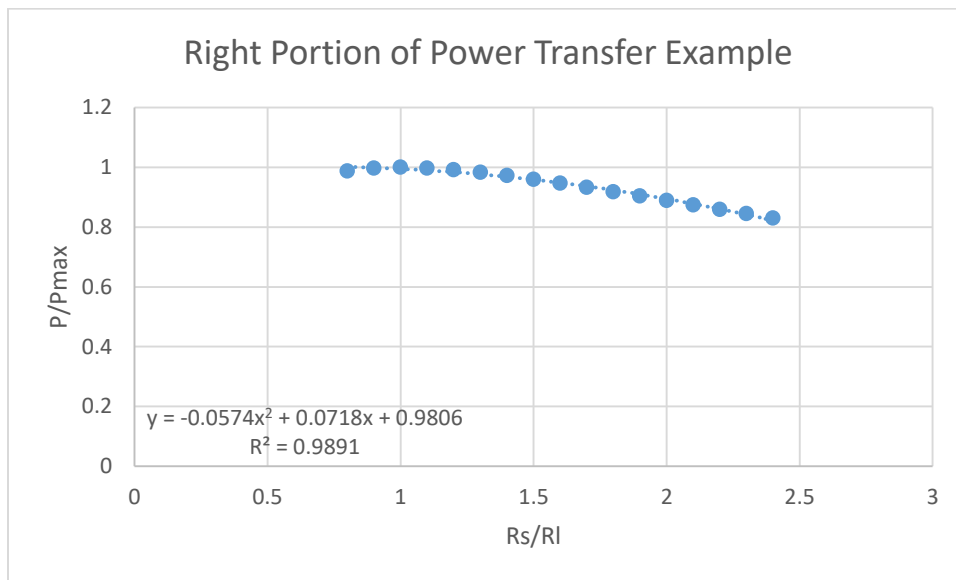


Figure 4.18: Right Portion of Power Transfer Example

4.2 Working Distance Analysis

Similar to the previous results found during the first stage of arc-flash testing, the measured amount of incident energy decreases significantly as working distance increases. Figure 4.19 depicts the relationship observed during the first stage of testing [1], [2]. Figure 4.20 depicts the relationship observed during the second stage of testing. Lastly, Figure 4.21 shows a comparison of the two relationships utilizing the common working distances among the two test stages. The trend exhibited by Figure 4.19 is approximate to the Inverse Square Law. By comparison, the trend in Figure 4.20 deviates more significantly from the Inverse Square Law. It is likely the deviation is due

to the second stage of testing utilizing a smaller range of working distances. If the working distance range in Figure 4.19 is limited to 15 inches, deviation from the Inverse Square Law increases. This change can be observed in Figure 4.21. Furthermore, Figure 4.21 shows that the shape of the trend lines generated over each stage of testing mirror each other closely. The faster decay exhibited by the trend line associated with the data collected during the second stage of testing is probably due to an interaction between the reduced range of working distances and the increase in system energy between test stages 1 and 2. Therefore, despite the increased deviation, the Inverse Square Law is a valid relationship to use for the results obtained in test stage two as it was in test stage 1.

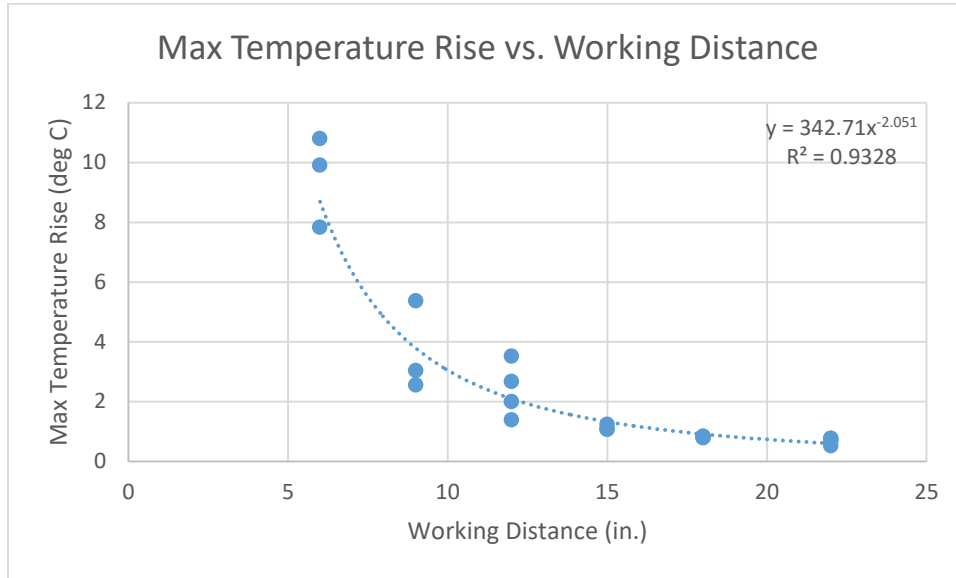


Figure 4.19: Max Temperature Rise vs. Working Distance for Stage 1 Tests

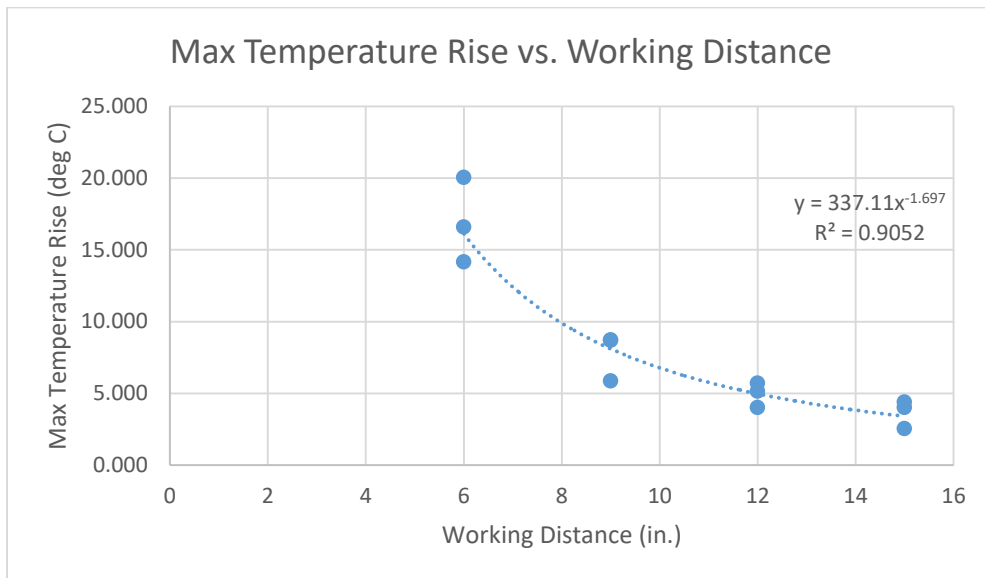


Figure 4.20: Max Temperature Rise vs. Working Distance for Stage 2 Tests

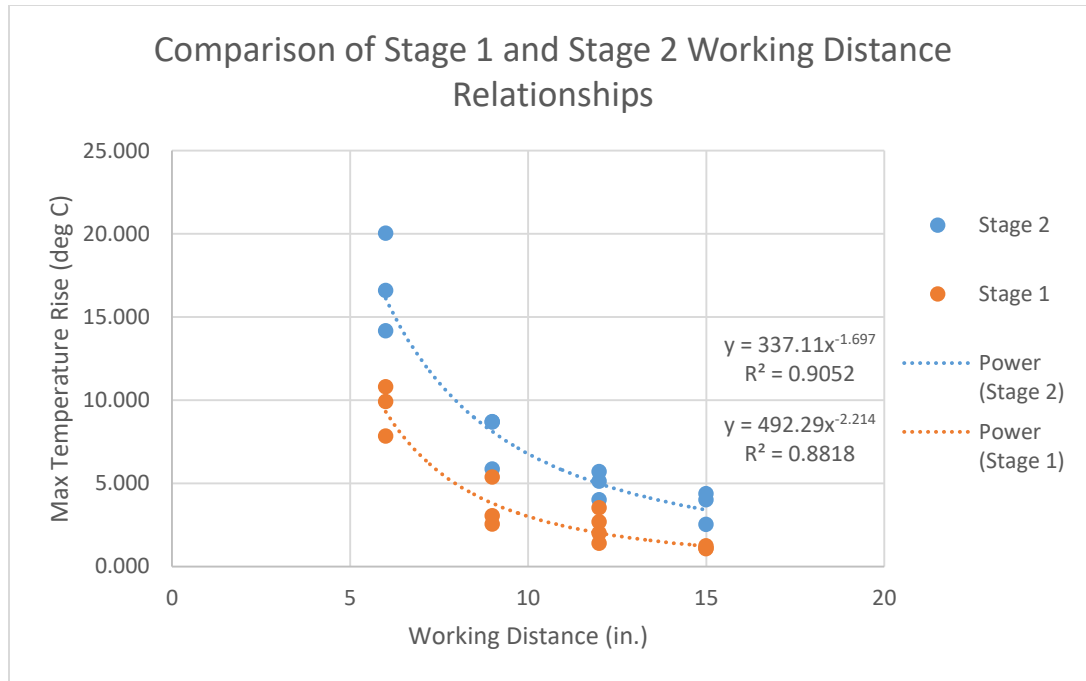


Figure 4.21: Comparison of Stage 1 and Stage 2 Working Distance Relationships

4.3 Arc Current Analysis

During the second stage of testing, the additional battery acquired possessed significantly greater capacity than either battery utilized during the first stage of testing (400 Ah vs. 100 Ah and 150 Ah). Thus, the battery increased the amount of available fault current to levels greater than that available during Test Stage 1. Furthermore, the battery was able to sustain an arc independently whereas the 100 Ah and 150 Ah batteries needed to be connected in parallel to sustain arcs consistently for the 200-millisecond test duration. This characteristic proved valuable once it was determined that Battery 1 was no longer usable. Since Battery 3 could be used independently, it was possible to acquire sufficient variation in current levels to allow an analysis between arcing currents and measured temperature rises.

Since gap width has a clear effect on arc current (see Figure 4.6 and Figure 4.7), it was necessary to divide data into categories based on gap width; thereby, producing Figure 4.22, Figure 4.23, Figure 4.24, and Figure 4.25. Three out of the four figures display a positive correlation between arc current and max temperature rise; however, the equation of the trend line differs among all three. By comparison, Figure 4.25, which corresponds with a 1/2-inch gap width, shows no clear relationship with data points being significantly scattered. This behavior may be due to the gap width being at the limit of arc sustainability, and as such, produces comparatively erratic arcs. Another interesting trend is displayed in Figure 4.26. Figure 4.26 depicts the relationship between average arc current and gap width for the two battery configurations. Unsurprisingly, the configuration utilizing Batteries 2 & 3 exhibits greater arc currents than the configuration utilizing solely Battery 3. The difference in average arc current between the two

configurations remains consistent as gap width increases until reaching a 1/2-inch gap width. At this point, the difference decreases dramatically with both configurations exhibiting an average arc current of approximately 3000 A. This behavior lends evidence to a 1/2-inch gap width being the maximum threshold of sustainability for 125 V_{DC}. It is unknown if greater capacity batteries at the same voltage level could overcome this limitation.

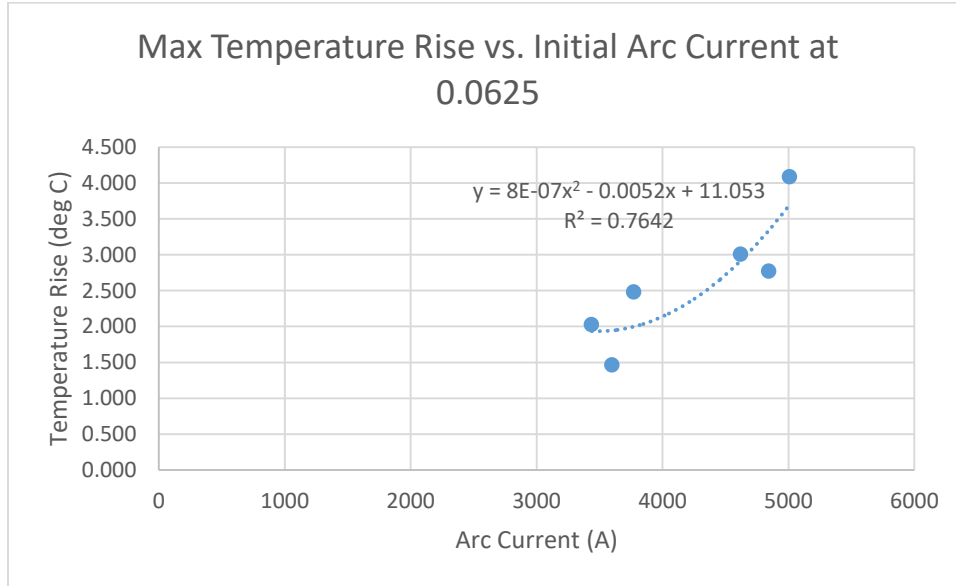


Figure 4.22: Max Temperature Rise vs. Initial Arc Current for a 1/16-inch Gap Width

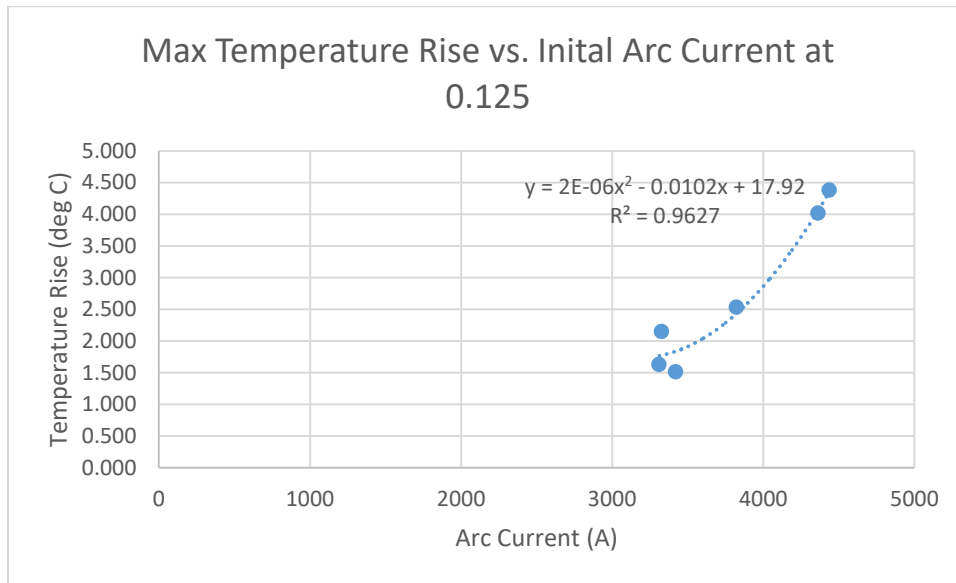


Figure 4.23: Max Temperature Rise vs. Initial Arc Current for a 1/8-inch Gap Width

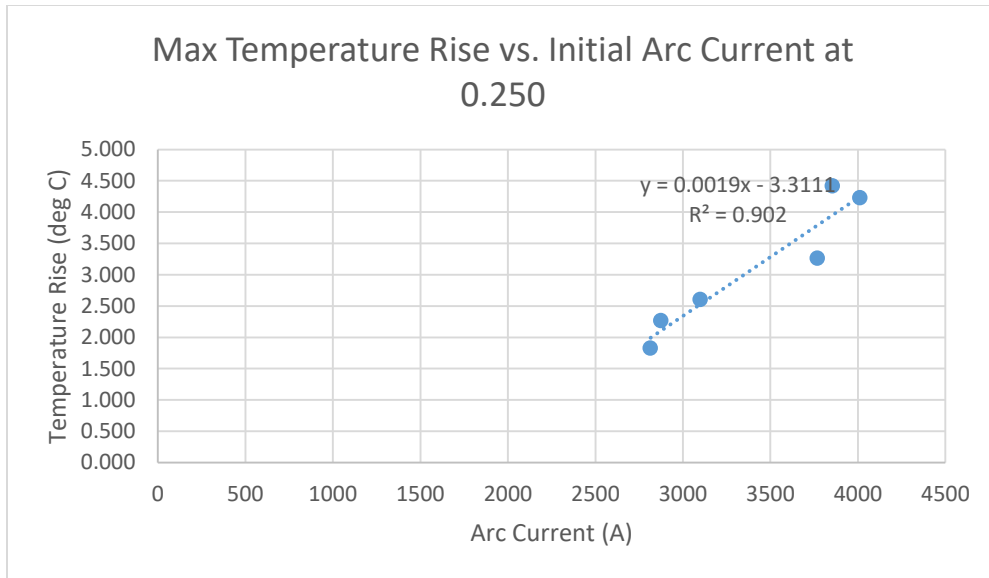


Figure 4.24: Max Temperature Rise vs. Initial Arc Current for a 1/4-inch Gap Width

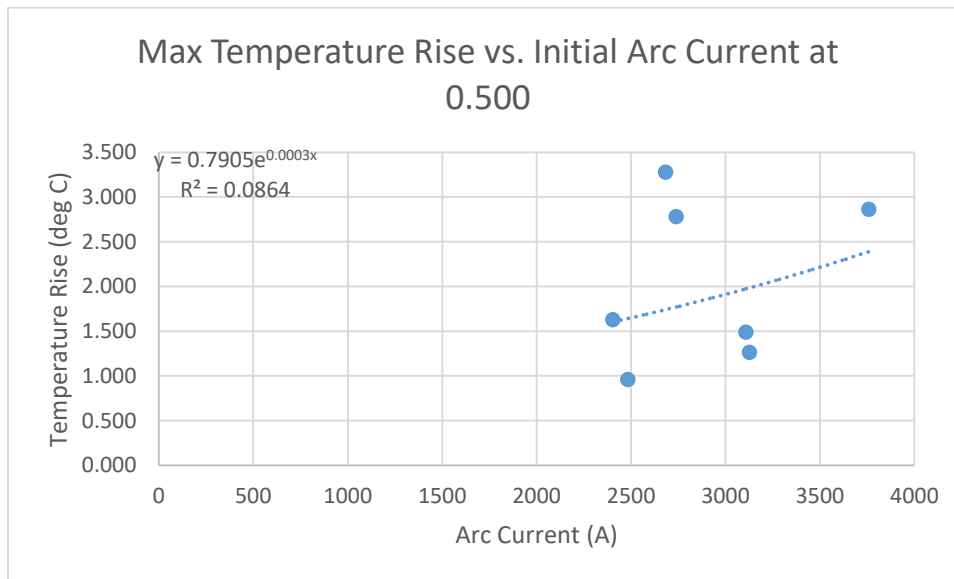


Figure 4.25: Max Temperature Rise vs. Initial Arc Current for a 1/2-inch Gap Width

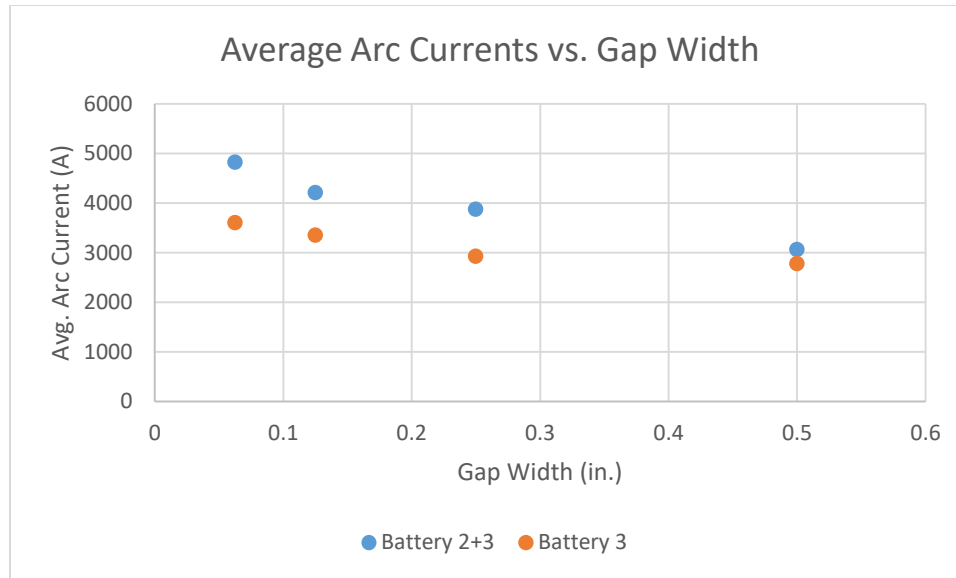


Figure 4.26: Average Arc Currents vs. Gap Width

4.4 Weather Data Analysis

Motivation for the weather analysis stems from an event that occurred during the 2018 testing. On August 8th, there was difficulty sustaining any arcs, even at gap widths that previously produced sustained arcs. It was hypothesized that atmospheric conditions may have resulted in the change in behavior since no other aspect of the test setup had been altered. An initial analysis utilizing weather data collected via a nearby weather station indicated that there was a statistically significant relationship between the duration of the arc and temperature, humidity, and pressure [2]. These findings were questionable and required further investigation due to the small sample size. Since there was no method to control atmospheric pressure, temperature and humidity were utilized as the independent variables for the weather tests. The primary measure of interest is arc duration; however, some analysis was performed with maximum temperature rise and average temperature rise serving as the dependent variables.

4.4.1 Relative Humidity

Relative humidity was investigated first due to a higher associated statistical significance in the initial statistical analysis. To begin, a series of graphs were generated to observe if any trends were apparent. These graphs were created based on temperature category. Dividing the relative humidity measurements among the temperature categories isolates the relative humidity relationships from possible interaction with temperature. Figure 4.27, Figure 4.28, and Figure 4.29 display the relative humidity graphs generated for medium temperature, high temperature, and low temperature, respectively. All three graphs pertaining to the relationship between arc duration and relative humidity depict trend lines with small slopes. The closer the slope of a trend line is to zero, the less likely the relationship is meaningful between the dependent and independent variables. Furthermore, the correlation coefficients (a.k.a. R-

values) are all less than 5% with the greatest magnitude being 4.86%. These low correlation coefficients provide additional evidence that there is no significant relationship between arc duration and relative humidity. Linear regression was performed for each data set to determine statistical significance. A fourth regression was performed utilizing data from all three temperature levels. The results are summarized in Table 4.1. It was found that humidity did not exhibit any statistically significant relationships with arc duration. Therefore, humidity does not significantly influence the sustainability of arcs.

Table 4.1: Arc Duration vs. Humidity Regression Results at Various Temperature Levels

Temperature	Parameter Estimate	P-value	Significant?
Low	0.000818	0.7504	No
Medium	-0.00103	0.5687	No
High	-0.000138	0.9338	No
All Levels	-0.0000445	0.9689	No

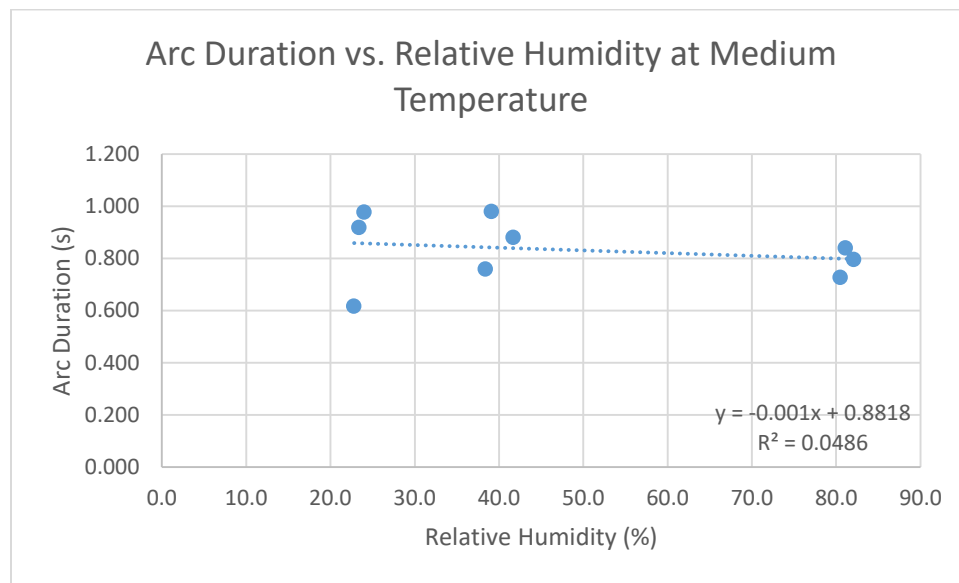


Figure 4.27: Arc Duration vs. Relative Humidity at Medium Temperature

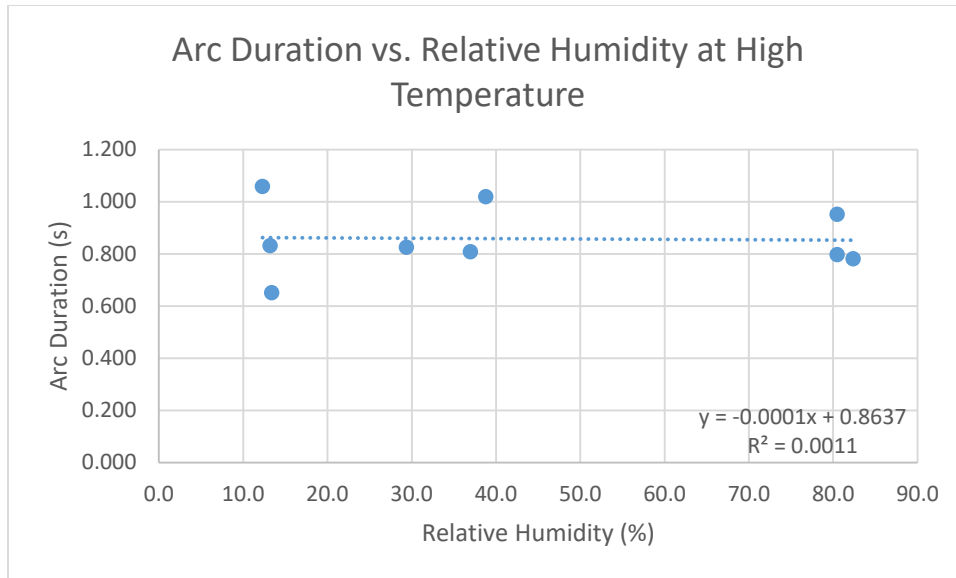


Figure 4.28: Arc Duration vs. Relative Humidity at High Temperature

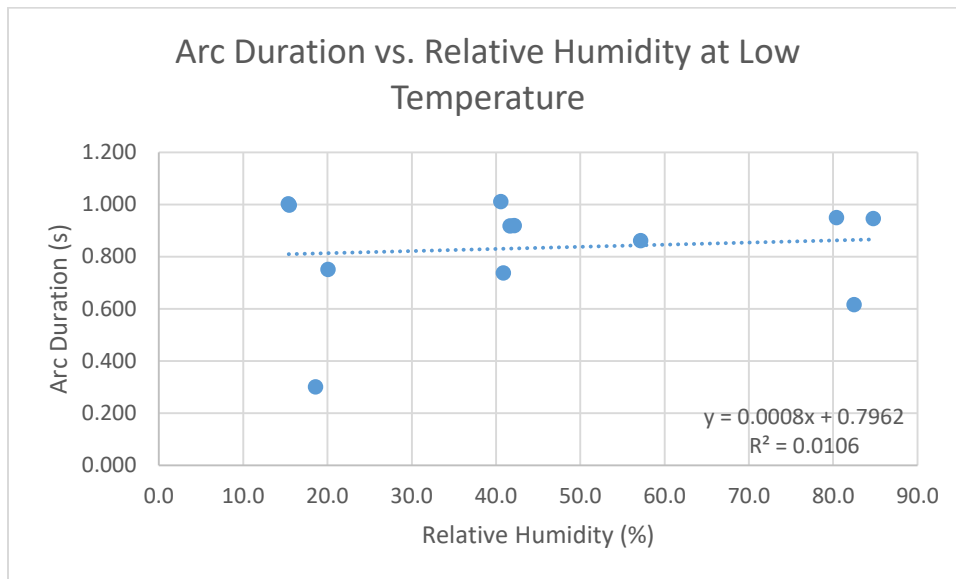


Figure 4.29: Arc Duration vs. Relative Humidity at Low Temperature

4.4.2 Temperature

The procedure utilized to analyze relationships between various arc characteristics and relative humidity was repeated for analyses involving environmental temperature. The key difference is that data was divided on the basis of relative humidity levels instead of temperature levels, as done before. Figure 4.30, Figure 4.31, and Figure 4.32 depict the relationships between arc duration and temperature at medium, high, and low relative humidity, respectively. Again, all three graphs display small slopes, which indicate that the two variables may be independent of one another. Furthermore, all three

figures exhibit low correlation coefficients. Performing a linear regression on each data set reveals that there is no significant correlation between arc duration and temperature at any of the three humidity levels as summarized in Table 4.2. A fourth regression was performed utilizing combined temperature data, regardless of humidity. Thus, temperature does not influence arc duration thereby environmental temperature does not affect arc sustainability.

Table 4.2: Arc Duration vs. Temperature Regression Results at Various Humidity Levels

Humidity	Parameter Estimate	P-value	Significant?
Low	0.00217	0.6664	No
Medium	-0.000208	0.9247	No
High	-0.000522	0.8568	No
All Levels	0.000685	0.7280	No

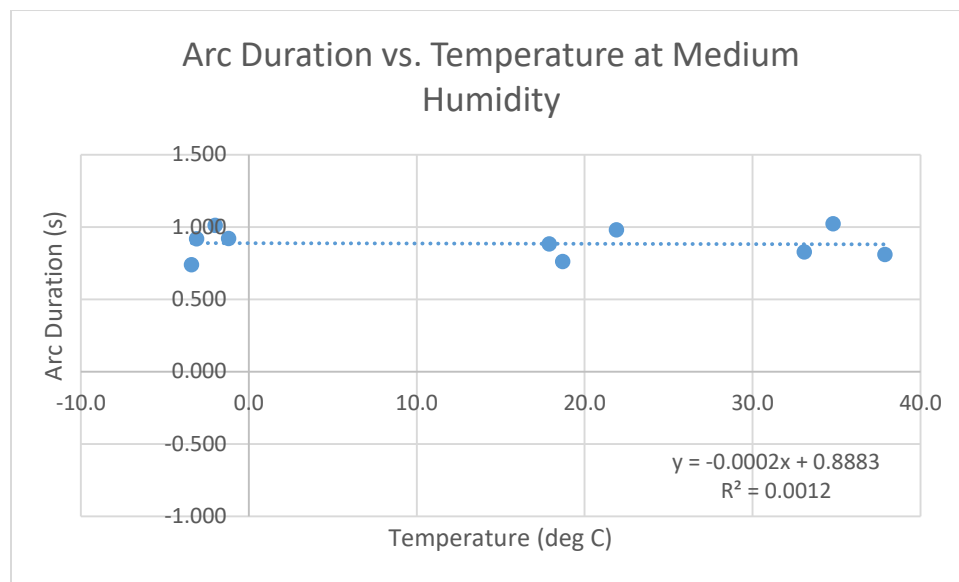


Figure 4.30: Arc Duration vs. Temperature at Medium Relative Humidity

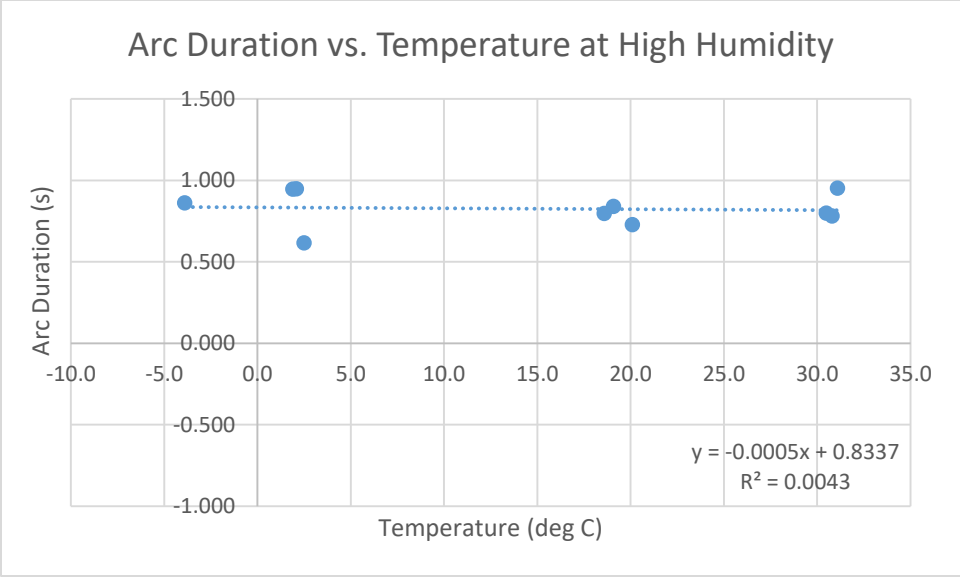


Figure 4.31: Arc Duration vs. Temperature at High Relative Humidity

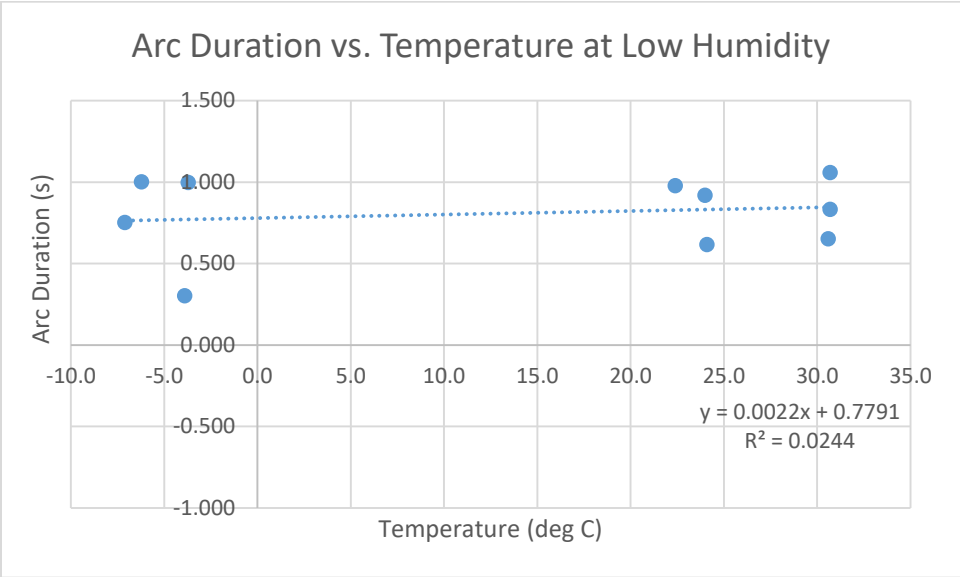


Figure 4.32: Arc Duration vs. Temperature at Low Relative Humidity

4.4.3 Air Pressure

Though air pressure was not controllable, regression analyses were performed utilizing air pressure. Each regression utilized a different data set and sought to find a relationship between arc duration and air pressure. One data set contained tests that utilized Batteries 2 and 3, another data set used tests that utilized only Battery 3, and the last data set used all available data. A summary of regression results is contained in Table 4.3. Based on the different regression results; there is no statistically significant relationship between arc duration and air pressure. However, given the small difference

between data points it is unknown how impactful these results are regardless of significance.

Table 4.3: Arc Duration vs. Air Pressure Regression Results

Data Set	Parameter Estimate	P-value	Significant?
All	0.549	0.0821	No
Battery 3	17.1	0.3037	No
Battery 2+3	0.222	0.3460	No

4.4.4 Multiple Linear Regression

The last major statistical analysis performed regarding weather data was a multiple linear regression of arc duration using temperature, humidity, pressure, and their interaction variables. For this analysis, the model was refined via the process of elimination. Therefore, after performing a regression analysis, the factor that exhibited the largest p-value (in other words, the least significant factor) was removed from the model and another regression was performed. As variables were eliminated, p-values and the adjusted R-square of the model were monitored for signs of improvement. The model was considered complete once all factors exhibited p-values less than 5% and no alterations could be made to improve the adjusted R-square value. If there was a situation where two factors had the same p-value, then one factor was selected randomly to eliminate except if one of the factors was an interaction term. Interaction terms were always eliminated before measured factors when p-values were equivalent. Following this procedure, the multiple linear regression model did not show statistical significance. Therefore, arc duration shows no statistical significant relationships with any atmospheric condition. A similar procedure was performed for peak and average temperature rise; however, air pressure and air pressure-related interaction terms were omitted. Similar to arc duration, neither model obtained statistical significance indicating that peak and average temperature rises are not significantly related with atmospheric conditions.

4.5 Chapter Summary

A number of different relationships were analyzed utilizing gap width as the independent variable. These relationships include maximum temperature rise, arc current, arc voltage, arc impedance, and arc energy. While the relationship between gap width and maximum temperature rise was consistent among the two battery configurations used, tests performed during the first stage of testing indicated that gap width and maximum temperature rise can produce conflicting results depending on working distance [2]. Therefore, the relationship between maximum temperature rise and gap width will not be used to develop a model due to interaction effects with working distance.

Similar to the maximum temperature rise relationship, the arc characteristic relationships (current, voltage, resistance) were approximate regardless of battery configurations. Furthermore, these relationships matched expectations with voltage

increasing, current decreasing, and resistance increasing as gap widths increased. For these three relationships, initial values were selected due to varying values occurring over the duration of the arc. This variance can be observed in Figure 4.3, Figure 4.4, and Figure 4.5. Overall, the arc characteristic relationships may be useful to derive a model.

In contrast to the other gap width relationships (maximum temperature rise, arc current, arc voltage, and arc resistance), arc energy exhibited two different trends depending on battery configuration. Despite their differences, both trends could be explained via the maximum power transfer theorem. Essentially, both trends belonged to the same relationship; however, where the trends began along the relationship varied based on system resistance, which changed between battery configurations. The existence of two relationships complicates usage of arc energy to develop a model for incident energy. Thus, assumptions may be necessary to use arc energy as a component of the final model.

Working distance displays a similar trend to that previously observed during the first stage of testing. Furthermore, working distance is still approximate to the Inverse Square Law. The exponent is less than that observed in the first test stage. This deviation is likely due to the range of working distance being reduced (15 inches in Stage 2 versus 22 inches in Stage 1). Comparing the working distance relationships of the first and second test stages, there is a consistent deviation between the two relationships, which may be attributable to the difference in fault current capabilities. This indicates that the relationship in Stage 2 would exhibit similar behavior to the relationship in Stage 1 if additional working distances were utilized. Therefore, this allows a greater understanding of how working distance interacts with temperature rise, and thereby, incident energy.

The arc current relationships were possible in Stage 2 because of the addition of Battery 3, which could generate sustainable arcs without being connected in parallel with another battery. The ability to sustain arcs independently of another battery allowed tests to be performed at different current levels; thereby, allowing the creation of these current relationships. Overall, arc current exhibited a positive correlation with maximum temperature rise; however, this correlation weakened as gap width increased until the relationship broke down at a 0.5-inch gap width. Furthermore, average arc currents were compared over the various gap widths. It was found that the deviation in average arc currents between the two battery configurations was consistent until a 0.5-inch gap width. This collapse in the profile coupled with the breakdown of the arc current and maximum temperature rise relationship provide additional evidence that a 0.5-inch gap width is approaching the limits of arc sustainability.

Lastly, analysis was performed to determine whether relative humidity, environmental temperature, or air pressure influences arc duration, maximum temperature rise, or average temperature rise. This analysis was performed due to the inability to sustain arcs on August 8th during the first stage of testing. Difficulty sustaining arcs was hypothesized to be the result of atmospheric conditions. A statistical

analysis of local weather data gave some credibility to this hypothesis. Therefore, tests during the second stage of testing were dedicated to determining the validity of these results in a more controlled manner. By observing the various graphical relationships and performing additional statistical analysis, it was determined that no statistically significant relationship exists between arc duration and the various environmental parameters.

CHAPTER 5: MODEL DEVELOPMENT

5.1 Discussion of DC Arc-flash Test Stage 1 Model

The equation developed during the first stage of testing is depicted in (12).

$$\frac{(C_f)(f(GW))(t)}{D^b} = E_{inc} \quad (12)$$

where:

C_f = correction factor

$f(GW)$ = a function of gap width (in)

t = arc duration (s)

D = working distance (in)

b = exponential term for working distance

E_{inc} = incident energy (cal/cm²)

The objective of (12) was to calculate incident energy by first calculating the arc energy in the numerator then adjusting the arc energy according to working distance and applying a correction factor that accounts for conversion factors and model fitting. This fundamental idea is represented in (13).

$$\frac{(C_f)(E_{arc})}{D^b} = E_{inc} \quad (13)$$

where:

E_{arc} = arc energy (cal)

The primary issue with the model developed during Stage 1 is that the relationship is confined to a single voltage and current level. For Stage 2 testing, a new battery was acquired, thereby allowing different current levels to be modeled. Thus, a new model must be defined to account for current relationships.

5.2 Development of DC Arc-flash Test Stage 2 Model

To account for a current relationship, arc energy must be redefined accordingly. Initial attempts to incorporate arc current into the model revisited the definition of electrical energy, which is depicted in (14).

$$E_{arc} = V_{arc}I_{arc}t = I_{arc}^2R_{arc}t = \frac{V_{arc}^2}{R_{arc}}t \quad (14)$$

where:

E_{arc} = arc energy (J)

V_{arc} = average arc voltage (V)

I_{arc} = average arc current (A)

t = arc duration (s)

Since arc duration was standardized for testing, a normalized arc energy was defined the same as arc power with additional terms for parameter estimates calculated during statistical analysis. The definition of normalized arc energy is provided in (15).

$$E_{arc,norm} = a(I_{arc}^2)(R_{arc}) \quad (15)$$

where:

$E_{arc,norm}$ = arc energy normalized at an arc duration of 0.2 seconds

a = model coefficient

By defining normalized arc energy in terms of arc current and arc resistance, it is necessary to provide definitions to relate arc characteristics to parameters that are easily measured or determined during normal operation conditions for practicality. Thus, two additional relationships were defined, the first of which is between gap width and arc resistance as depicted in (16).

$$R_{arc} = a(W_{gap}) + b \quad (16)$$

where:

W_{gap} = gap width (in.)

b = model intercept

The second relationship connects arc current to fuse current. An expression of this relationship is depicted in (17). The use of fuse current is based on the assumption that fuse current and fault current are analogous. Thus, fault current calculated based on system information should be roughly equivalent to fuse current.

$$I_{arc} = a(I_{fuse}) + b \quad (17)$$

where:

I_{fuse} = fuse current (A)

Once the normalized arc energy is determined, the peak incident energy is calculated via the same method as (13). Equation (18) shows the combined form of the model, where

$E_{arc,norm}$ is a function of two separate functions (one representing I_{arc} and another representing R_{arc}). In addition, a time factor is included to adjust for different arc durations. This time factor assumes a linear relationship between time and incident energy and accounts for the standardized test duration (200 ms or 0.2 seconds).

$$E_{inc} = \left(\frac{(C_f)(E_{arc,norm}(f(I_{fuse}), f(W_{gap})))}{D^b} \right) \left(\frac{t}{0.2} \right) \quad (18)$$

While performing statistical analyses to determine parameter estimates for equations (15), (16), and (17), two other models were developed. The first model is depicted in (19) and sought to establish a direct correlation between incident energy, arc current, and arc resistance. Establishing a more direct relationship was viewed favorably due to consolidation of equations and potential accuracy improvements.

$$E_{inc} = \left(\frac{a(I_{arc}^2)(R_{arc})}{D^b} \right) \left(\frac{t}{0.2} \right) \quad (19)$$

The second model is depicted in (20) and was created in an attempt to find a better model form to express incident energy. Originally, gap width was included as an additional term; however, it was shown to be statistically insignificant after performing a nonlinear regression analysis. Though the omission of gap width was viewed as undesirable, the model was still utilized for a comparative study to assess which model presented the best accuracy.

$$E_{inc} = \left(\frac{a(I_{fuse})}{D^b} \right) \left(\frac{t}{0.2} \right) \quad (20)$$

Three models were developed during the statistical analysis of the data. The first model is defined in (18), the second model is defined in (19), and the final model is defined in (20). Statistical characteristics of the first, second, and third models are summarized in Table 5.1. In addition, accuracy of the models was determined based on the average percent difference between calculated and measured incident energy. Model precision was assessed based on the standard deviation of percent differences. Percent difference is defined in

$$Percent\ Difference = \frac{E_{inc,predicted} - E_{inc,measured}}{E_{inc,measured}} (100\%) \quad (21)$$

where:

$E_{inc,predicted}$ = incident energy predicted/calculated (cal/cm²)

$E_{inc,measured}$ = incident energy measured during testing (cal/cm²)

Lastly, the conservatism of the models was analyzed based on the number of times that the model under-predicted the incident energy. A summary of accuracy measurements are provided in Table 5.2. These accuracy measurements were calculated using only test data associated with a working distance of 15 inches.

Table 5.1: Statistical Analysis Summary of Incident Energy Models

Model	Parameter	Estimate	p-value	Significant?
1	a	0.00845	<0.0001	Yes
	b	1.90	<0.0001	Yes
2	a	0.000329	0.0002	Yes
	b	0.115	<0.0001	Yes
3	a	0.0119	<0.0001	Yes
	b	1.87	<0.0001	Yes

Table 5.2: Summary of Model 1, 2, and 3 Accuracy Measurements

	Model 1	Model 2	Model 3
Average Percent Difference	51.3	51.8	33.6
Std. Dev. of Percent Differences	66.0	67.3	28.0
Under-predictions	14.0	14.0	9.00

Based on the results of the statistical analyses, all three models exhibited statistically significant parameter estimates. Therefore, the estimates provided and model forms can be utilized. In terms of overall performance, the third model (represented by (20)) was more accurate and precise than the other two models. In addition, Model 3 exhibited the fewest under-predictions, which means that the model is more conservative compared to Models 1 and 2. The primary concern with Model 3 is that the model only utilizes fuse current and working distance.

Based on previous research, gap width has been established as a significant parameter with respect to incident energy. The omission of gap width from the model is concerning. Therefore, additional research was performed to develop new models. These new models are inspired by the models developed in IEEE 1584-2002. Thus, instead of attempting an electrical theory approach (fitting nonlinear relationships based on fundamental definitions of electrical energy and power), a statistics-oriented approach was employed. This approach is characterized by using linear regression to establish relationships rather than fundamentals of electricity. Electrical theory is simply employed to identify which variables affect other variables.

A series of relationships was established based on this statistics-based approach. These relationships were used to design four new models. These models will be designated Models A, B, C, and D to distinguish them from the models developed via the electrical theory approach (Models 1, 2, and 3). The relationships that comprise these models are depicted in (22) through (27). Furthermore, parameter estimates are summarized in Table 5.3 through

Table 5.8. Some notes regarding these relationships:

1. Bolted fault current (I_{bf}) is used instead of fuse current (I_{fuse}) for (22) and (25). Previously, I_{fuse} was assumed to be equivalent to I_{bf} , however, testing showed that using predicted fault currents (calculated from battery manufacturer information) instead of fuse currents improved R-square values. Therefore, I_{bf} represents the fault current that would be calculated using battery manufacturer information. It should be noted that there was a discrepancy regarding manufacturer information on Battery 3. The pdf file originally provided with the battery indicated that the associated fault current was 4.1 kA. A separate information file found on the manufacturer's website shows the fault current as 4.5 kA [24]. It is likely that the file on the manufacturer's website is an updated version of the original pdf file. The 4.1 kA estimate was used to develop relationships. Using the lower fault current value increases conservatism of the model by relating higher incident energies with lower fault currents. This was viewed as a method to develop some form of safety factor to counteract the variability exhibited throughout arc-flash testing. It was deemed preferable to err on the side of caution when developing the relationships.
2. Equations (22) and (25) are specified in the same manner. The key difference between these two equations is that (22) relates the independent variables to arc current whereas (25) relates the same independent variables to arc energy. This was done to determine if the independent variables used to describe arc current could be used to describe arc energy instead, simplifying the total number of equations. Furthermore, it was found that the independent variables described arc energy better than arc current (this was assessed based on the R-square value).
3. The arc energy and normalized incident energy relationships displayed in (23) and (26), respectively, were developed based on elimination. The elimination procedure to develop a model begins with all possible parameters being incorporated into the model to define the desired variable. Afterwards, linear regression is performed to determine the statistical significance of the model parameters. The model parameter with the greatest p-value (or in other words, the least statistically significant parameter) is removed from the model and linear regression is repeated. This procedure is repeated until only statistically significant parameters remain in the model.
4. Equation (26) establishes incident energy normalized at a working distance of 15 inches. This normalized incident energy is then adjusted using the relationship established in (27). This approach is similar to IEEE 1584-2002. The exponent (b) is established by the relationship represented by (28).

$$I_{arc} = a(I_{bf}) + b(W_{gap}) + c(I_{bf} * W_{gap}) + d \quad (22)$$

where:

I_{bf} = bolted fault current (A)

$(I_{bf} * W_{gap})$ = interaction term for bolted fault current and gap width

b = model coefficient

c = model coefficient

d = model intercept

Table 5.3: Summary of Results for Arc Current vs. Bolted Fault Current, Gap Width, and Interaction Term

Adjusted R-square	Parameter	Estimate	p-value	Significant?
84.57%	<i>a</i>	0.483	<0.0001	Yes
---	<i>b</i>	1730	0.2170	No
---	<i>c</i>	-0.802	0.0020	Yes
---	<i>d</i>	1580	0.0030	Yes

$$E_{arc} = a(I_{arc}) + b(W_{gap}) + c \quad (23)$$

where:

c = model intercept

Table 5.4: Summary of Results for Arc Energy vs. Arc Current and Gap Width

Adjusted R-square	Parameter	Estimate	p-value	Significant?
71.14%	<i>a</i>	1.88	<0.0001	Yes
---	<i>b</i>	4840	<0.0001	Yes
---	<i>c</i>	-626	0.5233	No

$$E_{inc} = \frac{a(E_{arc})}{D^b} \quad (24)$$

Table 5.5: Summary of Results for Incident Energy vs. Arc Energy and Working Distance

Adjusted R-square	Parameter	Estimate	p-value	Significant?
94.40%	<i>a</i>	0.00845	<0.0001	Yes
---	<i>b</i>	1.90	<0.0001	Yes

$$E_{arc} = a(I_{bf}) + b(W_{gap}) + c(I_{bf} * W_{gap}) + d \quad (25)$$

Table 5.6: Summary of Results for Arc Current vs. Bolted Fault Current, Gap Width, and Interaction Term

Adjusted R-square	Parameter	Estimate	p-value	Significant?
90.53%	a	1.02	<0.0001	Yes
---	b	5510	0.0040	Yes
---	c	-0.995	0.0028	Yes
---	d	1590	0.0029	Yes

$$E_{inc,norm} = a(E_{arc}) + b \quad (26)$$

where:

$E_{inc,norm}$ = incident energy normalized at a working distance of 15 inches

Table 5.7: Summary of Results for Normalized Incident Energy vs. Arc Energy

Adjusted R-square	Parameter	Estimate	p-value	Significant?
70.42%	a	9.05×10^{-5}	<0.0001	Yes
---	b	-0.299	0.0029	Yes

$$E_{inc} = (E_{inc,norm}) \left(\frac{15^b}{D^b} \right) \quad (27)$$

$$E_{inc} = \left(\frac{a}{D^b} \right) \quad (28)$$

Table 5.8: Summary of Results for Incident Energy vs. Working Distance at a Gap Width of 0.125 Inches

Adjusted R-square	Parameter	Estimate	p-value	Significant?
91.15%	a	58.2	0.0288	Yes
---	b	1.81	<0.0001	Yes

Model A is developed via the following procedure. First, calculate arcing current by using (22). After calculating arcing current, arc energy is found via (23). Once arc energy has been determined, incident energy can be calculated using (24). Model B was developed by calculating arc energy via (25) and then using (24) to determine incident energy. Model C was developed by following the initial steps of Model A to determine arc energy. Afterwards, incident energy is calculated using a combination of (26) and (27). Lastly, Model D was developed by following the initial step of Model B to determine arc energy and then following the end steps of Model C to determine incident energy. Models A, B, C, and D are represented by (29), (30), (31), and (32),

respectively. Each model includes a time factor to account for different arc durations. In addition, a visual summary of the construction of each model is provided for clarity:

- Model A: (22) → (23) → (24)
- Model B: (25) → (24)
- Model C: (22) → (23) → (26) → (27)
- Model D: (25) → (26) → (27)

$$E_{inc} = \left(\frac{(C_f)(a(b(I_{bf}) + c(W_{gap}) + d(I_{bf} * W_{gap}) + e) + f(W_{gap}) + g)}{D^h} \right) \left(\frac{t}{0.2} \right) \quad (29)$$

$$E_{inc} = \left(\frac{(C_f)(a(I_{bf}) + b(W_{gap}) + c(I_{bf} * W_{gap}) + d)}{D^e} \right) \left(\frac{t}{0.2} \right) \quad (30)$$

$$E_{inc} = (a(b(c(I_{bf}) + d(W_{gap}) + e(I_{bf} * W_{gap}) + f) + g(W_{gap}) + h) + i) \left(\frac{15^j}{D^j} \right) \left(\frac{t}{0.2} \right) \quad (31)$$

$$E_{inc} = (a(b(I_{bf}) + c(W_{gap}) + d(I_{bf} * W_{gap}) + e) + f) \left(\frac{15^g}{D^g} \right) \left(\frac{t}{0.2} \right) \quad (32)$$

After establishing the new models, the same procedure used to assess Model 1, 2, and 3 was utilized. The results of the study are summarized in Table 5.9. Comparing the results of Table 5.9 with Table 5.2 indicates that the most accurate and precise model is Model D with an average percent difference of 23.27% and standard deviation of 17.70%. Thus, Model D was selected as the preferred model form.

Table 5.9: Summary of Model A, B, C, and D Accuracy Measurements

	Model A	Model B	Model C	Model D
Average Percent Difference	31.5	27.4	27.5	23.3
Std. Dev. of Percent Differences	30.4	25.6	26.7	17.7
Under-Predictions	11.0	9.00	14.0	11.0

5.3 Cross-Validation and Refinement of DC Arc-flash Test Stage 2 Model

To ensure the validity of Model D, cross-validation was performed using test results from DC Arc-flash Test Stage 1. The results of the cross-validation attempt are summarized in Table 5.10. Based on these results, Model D is deemed acceptable. The average percent difference was found to be 55.76%; therefore, the incident energies predicted by the model deviate from the measured incident energies by 55.76% on average. When using the data collected during DC Arc-flash Test Stage 2, the average

percent difference between the predicted and measured incident energies is 23.27%. Thus, Model D is less accurate when utilizing the Stage 1 data; however, Model D is conservative with only five under-predictions out of 36 tests.

Table 5.10: Summary of Cross-Validation Results

	Model D
Average Percent Difference	55.8
Std. Dev. of Percent Differences	38.1
Under-Predictions	5.00

The accuracy of Model D for the DC Arc-flash Test Stage 1 results can be improved by combining the data sets collected during both stages of testing. Thus, new parameter estimates were generated using a combined data set. A summary of parameter estimates is included in Table 5.11 and Table 5.12. Multiple relationships were assessed to see if adjusting the parameter estimates benefits the predictive capabilities of the model. It was determined that adjusting the parameter estimates for (25) and (26) provided the greatest benefit. In addition, it was found that calculating the parameter estimates from a combined dataset improved the overall fit of the relationships with the adjusted R-square values increasing for each. With updated parameter estimates, the average percent difference between the measured incident energy and predicted incident energy improved to 37.48%, which corresponds to a decrease of 18.28%. In addition, the associated standard deviation improved to 27.12%, which corresponds with a decrease of 11.00%. The improvement in accuracy and precision came at the cost of four additional under-predictions. Therefore, the refined model is not as conservative as the original; however, the model still over-predicted incident energy for most of the tests. Therefore, the refined model is still relatively conservative.

Table 5.11: Summary of Results for Refined Arc Energy vs. Bolted Fault Current, Gap Width, and Interaction Term

Adjusted R-square	Parameter	Estimate	p-value	Significant?
91.69%	A	1.19	<0.0001	Yes
---	B	7900	<0.0001	Yes
---	C	-1.32	<0.0001	Yes
---	D	364	0.2910	No

Table 5.12: Summary of Results for Refined Normalized Incident Energy vs. Arc Energy

Adjusted R-square	Parameter	Estimate	p-value	Significant?
72.39%	A	9.53×10^{-5}	<0.0001	Yes
---	B	-0.342	<0.0001	Yes

Table 5.13: Summary of Refined Model D Accuracy Measurements

	Refined Model D
Average Percent Difference	37.5
Std. Dev. of Percent Differences	27.1
Under-Predictions	9

5.4 Model Comparison

Lastly, Model D was compared with the DC Arc-flash Test Stage 1 model and the Ammerman model for open-air arc-flash. The open-air version of the Ammerman model was selected due to a comparison performed during the first stage of DC arc-flash testing that showed incident energy measurements matched the open-air form of the Ammerman model than the enclosure form of the Ammerman model [1]. The results of each model’s performance using the combined data set are summarized in Table 5.14. Out of the three models, the Ammerman model is the most accurate and precise with an average percent difference of 21.94% and associated standard deviation of 17.00%. The DC Arc-flash Test Stage 1 model was found to be the least accurate with an average percent difference of 35.52%. Model D was the least precise with a standard deviation of 23.87%. The Ammerman model under-predicted 37 (or approximately 53%) of the 70 observations used for comparison. The DC Arc-flash Test Stage 1 model was the least conservative with 53 under-predictions, which corresponds to approximately 76% of the tests being under-predicted. Conversely, Model D appeared the most conservative with only 28 under-predictions.

Table 5.14: Model Comparison Summary

	Model D	Stage 1	Ammerman
Average Percent Difference	30.1	35.5	21.9
Std. Dev. of Percent Differences	23.9	21.3	17.0
Under-Predictions	28.0	53.0	37.0

CHAPTER 6: CONCLUSION AND FUTURE WORK

A new model to describe DC arc-flash phenomena was successfully developed. The development of the model required a different approach than the methodology applied during DC Arc-flash Test Stage 1. The new methodology relied more on the precedence established by IEEE 1584-2002, which employed a more statistics-focused approach instead of relying on fundamental electrical theory. The new model is an improvement over the model proposed as a result of the first stage of DC arc-flash testing as the new model can account for different system fault currents. As for performance, the new model was shown to be more accurate than the DC Arc-flash Test Stage 1 model; however, the new model was noted as being less precise with a greater standard of deviation. When compared with the open-air version of the Ammerman model, the new model was shown to be more conservative. It should be noted that the Ammerman model was shown to possess greater accuracy and precision. One of the advantages of the new model is that it does not require an iterative approach; therefore, the new model is easier to utilize than the Ammerman model.

The behavior of the Ammerman model with the empirical dataset is promising. The semi-empirical nature of the Ammerman model has been proven to be effective in handling the empirical data gathered during these tests. Therefore, the Ammerman model is an effective tool for handling DC arc-flash system parameters outside the scope of the new model. To ensure conservative estimates, the enclosed version of the Ammerman model may be used. It should be noted that the enclosed version of the Ammerman model can result in poor predictions at very close distances (such as 6 inches). For these instances, using the open-air version of the Ammerman model may be more appropriate.

Lastly, with respect to atmospheric conditions, it was found that atmospheric conditions do not have a significant effect when assessed based on arc duration alone. The focus on arc duration is because arcs were difficult to sustain during the first stage of testing on August 8th, 2018. Thus, arc duration became the primary consideration for testing. There may be an effect with respect to the thermal rise measurements; however, that was outside the scope of testing. It should be noted that the test setup differed from that utilized during the previous stage of testing due to the failure of Battery 1. Therefore, these results can only be applied to the battery configurations utilized. Thus, the possibility that atmospheric conditions negatively affected the test setup during the first stage of DC arc-flash testing is still valid. However, based on the results gathered during the second stage of testing, the magnitude of the effect, if there were one, was likely small.

Though a new model was generated, there is still a need for additional research regarding DC arc-flash to create improved models and develop a greater understanding of the arcing phenomenon in DC systems. Considerations for future work include collecting more measurements, expanding the model, and applying additional modeling techniques to refine the model parameter estimates. The collection of additional measurements would allow the relationships to be refined and defined with greater certainty. Expansion

of the model could be pursued via the number of different methods. Some considerations that could expand the model would be to test batteries of different voltage levels, current capacities, and material composition. In addition, different test setups should be tested. Some examples include different electrode configurations, electrode shapes, and enclosure dimensions. Lastly, refinement of the model parameter estimates could be achieved by applying different statistical methods, such as k-fold cross-validation.

APPENDIX

Table A.1: Gap Width Analysis Data Table (Batteries 2 +3)

Test Name	Gap Width (in)	Fuse Current (A)	Arc Voltage Initial (V)	Arc Current Initial (A)	Arc Impedance Initial (ohms)	Arc Energy (cal)	Max Temp. Rise (deg C)
HBDC Arc_125_08	0.125	5023	39.60	3822	0.01036	7905.6	2.533
HBDC Arc_125_09	0.125	5660	43.39	4438	0.00978	8801.9	4.379
HBDC Arc_125_10	0.125	5382	41.88	4363	0.00960	8710.8	4.014
HBDC Arc_250_011	0.250	4386	55.21	3768	0.01465	8874.3	3.265
HBDC Arc_250_012	0.250	4573	47.11	4012	0.01174	8840.8	4.230
HBDC Arc_250_013	0.250	5707	51.82	3854	0.01345	8900.6	4.416
HBDC Arc_062_014	0.063	5379	38.11	4621	0.00825	8600.2	3.008
HBDC Arc_062_015	0.063	5666	36.64	5009	0.00731	8552.8	4.086
HBDC Arc_062_016	0.063	5452	40.53	4844	0.00837	8809.5	2.772
HBDC Arc_500_017	0.500	5412	74.12	3759	0.01972	8386.0	2.859
HBDC Arc_500_018	0.500	3847	80.38	2739	0.02935	7117.4	2.778
HBDC Arc_500_020	0.500	4458	72.23	2684	0.02691	7876.4	3.275

Table A.2: Gap Width Analysis Data Table (Battery 3 Only)

Test Name	Gap Width (in)	Fuse Current (A)	Arc Voltage Initial (V)	Arc Current Initial (A)	Arc Impedance Initial (ohms)	Arc Energy (cal)	Max Temp. Rise (deg C)
HBDC Arc_250_066	0.250	4404	54.10	3099	0.01746	6252.4	2.602
HBDC Arc_250_067	0.250	4408	50.06	2815	0.01778	6281.1	1.827
HBDC Arc_250_068	0.250	4353	49.30	2875	0.01715	6359.9	2.264
HBDC Arc_250_069	0.063	4449	32.55	3598	0.00905	5743.3	1.463
HBDC Arc_250_070	0.063	4438	35.54	3772	0.00942	5724.2	2.480
HBDC Arc_250_071	0.063	4483	35.92	3437	0.01045	5877.2	2.025
HBDC Arc_250_072	0.125	4464	37.27	3311	0.01126	5898.7	1.630
HBDC Arc_250_073	0.125	4412	37.55	3420	0.01098	5910.6	1.515
HBDC Arc_250_074	0.125	4470	40.06	3328	0.01204	6054.0	2.151
HBDC Arc_250_075	0.500	4402	71.73	3109	0.02307	6434.0	1.485
HBDC Arc_250_076	0.500	4404	66.99	3127	0.02142	6505.7	1.261
HBDC Arc_250_077	0.500	4355	69.24	2484	0.02787	3365.2	0.958
HBDC Arc_250_078	0.500	4385	65.03	2405	0.02704	6340.8	1.627

Table A.3: Arc Current Analysis Data Table

Test Name	Batteries Used	Gap Width (in)	Fuse Current (A)	Arc Current Initial (A)	Max Temp. Rise (deg C)	Peak Incident Energy (cal/sq. cm)
HBDC Arc_062_014	2+3	0.063	5379	4621	3.008	0.4061
HBDC Arc_062_015	2+3	0.063	5666	5009	4.086	0.5516
HBDC Arc_062_016	2+3	0.063	5452	4844	2.772	0.3742
HBDC Arc_250_069	3	0.063	4449	3598	1.463	0.1975
HBDC Arc_250_070	3	0.063	4438	3772	2.480	0.3348
HBDC Arc_250_071	3	0.063	4483	3437	2.025	0.2734
HBDC Arc_125_008	2+3	0.125	5023	3822	2.533	0.3420
HBDC Arc_125_009	2+3	0.125	5660	4438	4.379	0.5912
HBDC Arc_125_010	2+3	0.125	5382	4363	4.014	0.5419
HBDC Arc_250_072	3	0.125	4464	3311	1.630	0.2201
HBDC Arc_250_073	3	0.125	4412	3420	1.515	0.2045
HBDC Arc_250_074	3	0.125	4470	3328	2.151	0.2904
HBDC Arc_250_011	2+3	0.250	4386	3768	3.265	0.4408
HBDC Arc_250_012	2+3	0.250	4573	4012	4.230	0.5711
HBDC Arc_250_013	2+3	0.250	5707	3854	4.416	0.5962
HBDC Arc_250_066	3	0.250	4404	3099	2.602	0.3513
HBDC Arc_250_067	3	0.250	4408	2815	1.827	0.2466
HBDC Arc_250_068	3	0.250	4353	2875	2.264	0.3056
HBDC Arc_500_017	2+3	0.500	5412	3759	2.859	0.3860
HBDC Arc_500_018	2+3	0.500	3847	2739	2.778	0.3750

Test Name	Batteries Used	Gap Width (in)	Fuse Current (A)	Arc Current Initial (A)	Max Temp. Rise (deg C)	Peak Incident Energy (cal/sq. cm)
HBDC Arc_500_020	2+3	0.500	4458	2684	3.275	0.4421
HBDC Arc_250_075	3	0.500	4402	3109	1.485	0.2005
HBDC Arc_250_076	3	0.500	4404	3127	1.261	0.1702
HBDC Arc_250_077	3	0.500	4355	2484	0.958	0.1293
HBDC Arc_250_078	3	0.500	4385	2405	1.627	0.2196

Table A.4: Average Arc Current Data Table

Gap Width (in)	Avg. Arc Current (A)	
	Batt 2 + 3	Batt 3
0.063	4825	3602
0.125	4208	3353
0.250	3878	2930
0.500	3061	2781

Table A.5: Working Distance Analysis Data Table (Batteries 2 & 3)

Test Name	Gap Width (in)	Working Distance (in)	Max Temp. Rise (deg C)	Peak Incident Energy (cal/cm²)
HBDC Arc_125_08	0.125	15	2.533	0.3420
HBDC Arc_125_09	0.125	15	4.379	0.5912
HBDC Arc_125_010	0.125	15	4.014	0.5419
HBDC Arc_125_028	0.125	12	4.003	0.5404
HBDC Arc_125_029	0.125	12	5.130	0.6926
HBDC Arc_125_030	0.125	12	5.699	0.7694
HBDC Arc_125_031	0.125	9	8.699	1.1744
HBDC Arc_125_032	0.125	9	8.679	1.1717
HBDC Arc_125_033	0.125	9	5.853	0.7902
HBDC Arc_125_034	0.125	6	20.032	2.7043
HBDC Arc_125_035	0.125	6	14.156	1.9111
HBDC Arc_125_036	0.125	6	16.587	2.2392

Table A.6: Weather Analysis Data Table

Test Name	Batteries Used	Env. Temp. (deg C)	Temp. Cat.	Rel. Humid. (%)	Humid. Cat.	Air Pressure (in Hg)	Arc Duration (s)
HBDC Arc_250_021	2+3	30.7	High	12.3	Low	30.44	1.058
HBDC Arc_250_022	2+3	30.7	High	13.2	Low	30.43	0.831
HBDC Arc_250_024	2+3	30.6	High	13.4	Low	30.41	0.651
HBDC Arc_250_052	2+3	30.5	High	80.5	High	30.27	0.797
HBDC Arc_250_053	2+3	30.8	High	82.4	High	30.27	0.780
HBDC Arc_250_057	2+3	31.1	High	80.5	High	30.44	0.951
HBDC Arc_250_046	2+3	33.1	High	29.4	Med	30.42	0.825
HBDC Arc_250_049	2+3	34.8	High	38.8	Med	30.24	1.019
HBDC Arc_250_051	2+3	37.9	High	37.0	Med	30.27	0.808
HBDC Arc_250_037	2+3	-3.9	Low	18.6	Low	30.20	0.300
HBDC Arc_250_047	2+3	-6.2	Low	15.4	Low	30.33	1.001
HBDC Arc_250_048	2+3	-7.1	Low	20.1	Low	30.24	0.750
HBDC Arc_250_050	2+3	-3.7	Low	15.5	Low	30.27	0.996
HBDC Arc_250_058	2+3	-3.9	Low	57.2	High	30.43	0.860
HBDC Arc_250_059	2+3	1.9	Low	84.8	High	30.32	0.945
HBDC Arc_250_060	2+3	2.5	Low	82.5	High	30.32	0.615
HBDC Arc_250_061	2+3	2.1	Low	80.4	High	30.37	0.948
HBDC Arc_250_038	2+3	-3.4	Low	40.9	Med	30.40	0.736
HBDC Arc_250_039	2+3	-2.0	Low	40.6	Med	30.42	1.010
HBDC Arc_250_040	2+3	-3.1	Low	41.7	Med	30.42	0.917

Test Name	Batteries Used	Env. Temp. (deg C)	Temp. Category	Rel. Humid. (%)	Humid. Category	Air Pressure (in Hg)	Arc Duration (s)
HBDC Arc_250_041	2+3	-1.2	Low	42.2	Med	30.44	0.918
HBDC Arc_250_083	3	21.0	Med	16.9	Low	30.15	1.315
HBDC Arc_250_080	3	20.9	Med	17.2	Low	30.15	0.132
HBDC Arc_250_081	3	20.8	Med	17.1	Low	30.15	0.568
HBDC Arc_250_082	3	20.9	Med	17.0	Low	30.15	0.836
HBDC Arc_250_084	3	21.2	Med	16.9	Low	30.11	0.027
HBDC Arc_250_025	2+3	22.4	Med	24.0	Low	30.03	0.977
HBDC Arc_250_026	2+3	24.1	Med	22.8	Low	30.05	0.616
HBDC Arc_250_027	2+3	24.0	Med	23.4	Low	30.03	0.918
HBDC Arc_250_054	2+3	20.1	Med	80.5	High	30.43	0.727
HBDC Arc_250_055	2+3	18.6	Med	82.1	High	30.43	0.795
HBDC Arc_250_056	2+3	19.1	Med	81.1	High	30.44	0.839
HBDC Arc_250_042	2+3	17.9	Med	41.7	Med	30.44	0.880
HBDC Arc_250_043	2+3	21.9	Med	39.1	Med	30.44	0.979
HBDC Arc_250_045	2+3	18.7	Med	38.4	Med	30.44	0.759

REFERENCES

- [1] A. C. Gaunce, X. Wu, J. D. Mandeville, D. J. Hoffman, A. Khalsa, J. Sottile and R. J. Wellman, "DC Arc Flash: Testing and Modeling Incidents in a 125V Substation Battery Backup System," in *IEEE Transactions on Industry Applications*.
- [2] A. C. Gaunce, "PREDICTIVE MODELING OF DC ARC FLASH IN 125 VOLT SYSTEM," *Theses and Dissertations--Mining Engineering*, vol. 46, 2019.
- [3] R. H. Lee, "The Other Electrical Hazard: Electric Arc Blast Burns," *IEEE Transactions on Industry Applications*, Vols. IA-18, no. 3, pp. 246-251, May 1982.
- [4] K. Kowalski-Trakofler and E. Barrett, "Reducing Non-Contact Electric Arc Injuries: An Investigation of Behavioral and Organizational Issues," *Journal of Safety Research*, vol. 38, pp. 597-608, 2007.
- [5] Electrical Safety Foundation International (ESFI), "Workplace Fatalities and Injuries 2003 - 2018," ESFI, 30 January 2020. [Online]. Available: <https://www.esfi.org/resource/workplace-fatalities-and-injuries-2003-2018-750>. [Accessed 22 March 2020].
- [6] R. B. Campbell and D. A. Dini, "Occupational Injuries From Electrical Shock and Arc Flash Events," The Fire Protection Research Foundation, Quincy, Massachusetts, U.S.A. , 2015.
- [7] B. D. Arnoldo, G. F. Purdue, K. Kowalske, P. A. Helm, A. Burris and J. L. Hunt, "Electrical Injuries: A 20-Year Review," *Journal of Burn Care Rehabilitation*, vol. 25, pp. 479-484, 2004.
- [8] J. Phillips, "IEEE 1584 - Changes to the Next Edition," brainfiller, 19 November 2018. [Online]. Available: <https://brainfiller.com/brainfiller-library/arc-flash-electrical-safety/ieee-1584-changes-in-the-next-edition/>. [Accessed 22 March 2020].
- [9] IEEE Guide for Performing Arc-Flash Hazard Calculations, IEEE 1584, 2002.
- [10] R. F. Ammerman, P. K. Sen and J. P. Nelson, "Electrical Arcing Phenomena: A historical perspective and comparative study of the standards IEEE 1584 and NFPA 70E," *Industry Applications Magazine*, pp. 42-52, May/June 2009.
- [11] J. Phillips, "How Did We Get Here," *Electrical Contractor*, May 2009. [Online]. Available: <https://www.ecmag.com/section/safety/how-did-we-get-here>. [Accessed 21 March 2020].

- [12] D. R. Doan, "Arc Flash Calculations for Exposures to DC Systems," *IEEE Transactions on Industry Applications*, vol. 46, no. 6, pp. 2299-2302, November/December 2010.
- [13] R. F. Ammerman, T. Gammon, P. K. Sen and J. P. Nelson, "DC-Arc Models and Incident-Energy Calculations," *IEEE Transactions on Industry Applications*, vol. 46, no. 5, pp. 1810-1819, September/October 2010.
- [14] A. D. Stokes and W. T. Oppenlander, "Electric arcs in open air," *Journal of Physics D: Applied Physics*, vol. 24, no. 1, pp. 26-35, 1991.
- [15] R. Wilkins, "Simple improved equations for arc flash hazard analysis," 30 Aug. 2004. [Online]. Available: <https://www.ieee.comunities.org/ieee.esafety>.
- [16] M. D. Fontaine and P. Walsh, "DC Arc Flash Calculations - Arc-in-open-air & Arc-in-a-box - Using a Simplified Approach (Multiplication Factor Method)," in *IEEE IAS Electrical Safety Workshop*, Daytona Beach, FL, USA, 2012.
- [17] S. H. Rau, Z. Zhang and W. J. Lee, "3-D Magnetohydrodynamic Modeling of DC Arc in Power System," *IEEE Transactions on Industry Applications*, vol. 52, no. 6, pp. 4549-4555, November/December 2016.
- [18] C. Keyes and C. Maurice, "DC Arc Hazard Assessment Phase II (K-012623-RA-0002-R00)," Kinectrics Inc., Toronto, Ontario, CA, 2007.
- [19] J. G. Hildreth and K. Feeney, "Arc Flash Hazards of 125 Vdc Station Battery Systems," *2018 IEEE Power & Energy Society General Meeting (PESGM)*, pp. 1-5, 2018.
- [20] IEEE Recommended Practice for the Design of DC Auxiliary Systems for Generating Stations, IEEE 946, 2004.
- [21] R. Wilkins, M. Lang and M. Allison, "Effect of Insulating Barriers in Arc Flash Testing," *IEEE Transactions on Industry Applications*, vol. 44, no. 5, pp. 1354-1359, 2008.
- [22] K. Gray, S. Robert and T. L. Gauthier, "Low Voltage 100-500 Vdc Arc Flash Testing," *2020 IEEE IAS Electrical Safety Workshop*, pp. 90-96, 2020.
- [23] J. D. Mandeville, "DC Arc Flash Instrumentation Report (PTS 213769.001)," AEP, Columbus, OH, 2019.
- [24] BAE, "BAE OGi-2V Cell (400-2400Ah Data Sheet)," [Online]. Available: <https://www.baebatteriesusa.com/ogi-2v-cell/>. [Accessed 30 March 2020].

VITA

Austin Cody Gaunce

Education:

University of Kentucky

Bachelor of Science in Mining Engineering	May 2016
Power and Energy Institute of Kentucky (PEIK) Graduate Certificate	Dec. 2017
Master of Science in Mining Engineering	May 2019

Work Experience:

Student Intern, American Electric Power, New Albany, OH

May 29 - August 17, 2018; January 1 - May 17, 2019

Engineer Associate, American Electric Power, New Albany, OH

May 18, 2019 - Present

Honors and Awards:

Central Appalachian Education Research Center (ERC) Graduate Fellowship

Certifications:

Engineer-in-Training (EIT) – Kentucky and Ohio